An Investigation of the DNA Interactions of Polyamine Anthracene Conjugates under High Ionic Conditions

Khoa Nguyen
knguyen68@gsu.edu

Follow this and additional works at: https://scholarworks.gsu.edu/chemistry_theses

AN INVESTIGATION OF THE DNA INTERACTIONS OF POLYAMINE ANTHRACENE

CONJUGATES UNDER HIGH IONIC CONDITIONS

by

KHOA T. NGUYEN

Under the Direction of Kathryn B. Grant, Ph.D.

ABSTRACT

Six polyamine anthracene conjugates (Ants) were studied that take advantage of the polyamine transporter system (PTS) to target specific cancer. The structural features of the Ants involve planar aromatic anthracene that has highly cytotoxicity properties and a polyamine chain similar to natural polyamine, which is taken up by eukaryote cells expressing the PTS actively. Experimental data show that Ants with di-substituted polyamine chains have significantly higher DNA binding affinities than the mono-substituted anthracene conjugates. The high ionic conditions (~150 mM NaCl and 260 mM KCl) in the eukaryote cell nucleus extensively impair the apparent DNA binding of the Ants, but may further reinforce DNA structural stability. Combining the published cytotoxicity of the PTS data with the DNA interaction data reported here, the di-substituted polyamine anthracene conjugates have the highest potential to, after cellular uptake via PTS, bind to DNA.

INDEX WORDS: polyamine anthracene conjugate (Ant), polyamine, polycyclic aromatic hydrocarbon, DNA binding constant (K), DNA binding mode, high ionic strength

AN INVESTIGATION OF THE DNA INTERACTIONS OF POLYAMINE ANTHRACENE

CONJUGATES UNDER HIGH IONIC CONDITIONS

by

KHOA T. NGUYEN

A Thesis Submitted in Partial Fulfillment of the Requirements for the Degree of

Master of Science

in the College of Arts and Sciences

Georgia State University

2016

AN INVESTIGATION OF THE DNA BINDING AFFINITY OF

POLYAMINE ANTHRACENE CONJUGATES UNDER HIGH IONIC CONDITIONS

by

KHOA T. NGUYEN

Committee Chair: Kathryn B. Grant

Committee: Dabney Dixon

Donald Hamelberg

Electronic Version Approved:

Office of Graduate Studies

College of Arts and Sciences

Georgia State University

December 2016

DEDICATION

To my family and friends, to my past, and to my future self.

ACKNOWLEDGEMENTS

To Dr. Grant, thank you for your advice and patience during these long years.

To my lab mates, Andy, Arash, Carla, Christina, Dominique, Kanchan, Kaitlyn, Tayabeh, Stephen, Sadegh, and Ziyi, thank you for your help and support, as well as advice on cooking.

To Brandford Adobaw, without your advice and the drive to do research, I would have lost my way.

To my committee members, thank you for your valuable time and advice in attending my thesis defense and reviewing my thesis.

TABLE OF CONTENTS

LIST OF TABLES

LIST OF FIGURES

1   INTRODUCTION

1.1   Polyamines and polycyclic aromatic hydrocarbons

1.1.1   Cancer

An uncontrollable growth of defective tumor cells is referred to as cancer. Many functional receptors, such as the ones responsible for cell growth regulation, are missing; the lack of these receptors results in the absence of cell apoptosis, or programmed cell death.[1] These cancer cells can inhibit healthy cells and organs from performing their normal functions. If left untreated, the cells of the growing tumor can detach, spread, and grow in other parts of the body, which is known as metastasis.[1] Treatments are available to combat the growth of cancer cells, such as surgery, radiation therapy, immunotherapy, and chemotherapy. The approach to treatment depends on the doctor and patient.[1, 2, 3] The uncontrollable growth requires a significant amount of nutrients for the cancer cells; the design for anti-cancer drugs has taken advantage of this increased uptake to be included in their drug delivery strategies.

1.1.2   Polycyclic aromatic hydrocarbons

As the name implies, polycyclic aromatic hydrocarbons (PAHs) consist of multiple fused aromatic hydrocarbon rings. PAHs are byproducts from coal tars, cigarette smoke, car exhaust, etc. and are considered pollutants.[4, 5] Furthermore, PAHs are toxic and a health hazard due to their carcinogenic, mutagenic, and teratogenic activities even at low levels.[5, 6, 7] The earliest report about the carcinogenic characteristics of PAHs was on chimney sweepers circa 1775, whose jobs required constant contact with smokes and ashes; they later developed skin and scrotum cancer.[8] PAHs can form DNA adducts by creating a wedge between two DNA base pairs, also known as intercalation.[9] In the body, the PAHs can be converted to other cytotoxic

metabolites, such as the diol-epoxides.[10] These diol-epoxide PAHs can covalently bind to the purine bases, adenine and guanine, to form a stable DNA adduct.[11] The structural perturbation of the DNA helix caused by the DNA adducts can prevent the binding of polymerases, which can interfere with transcription and replication. Furthermore, PAHs can redox cycle to produce reactive oxygen species (ROS) that can induce oxidative stress.[11] Anthraquinone, an oxidative derivative of the PAH anthracene, acts as a DNA replication and transcription inhibitor by binding tightly to the DNA duplex.[12, 13] Many PAHs can be derived and utilized in medicinal and the industrial fields. For example, anthracene and its derivatives are employed as fluorescence materials,[14] precursors for dye,[15] and anti-cancer agents.[16, 17, 18] An example is mitoxantrone, an anthraquinone and an FDA-approved anti-cancer drug.[19]

1.1.3   *Uptake of the polyamine compounds*

Polyamines are involved in multiple cellular processes, including cell growth and cell replication. Thus, cells have developed mechanisms to control the uptake of these compounds.[20, 21] Polyamines, such as spermine, are protonated under physiological conditions and can contribute to an active interaction with the negative phosphodiester backbone of DNA. [20, 21, 22] The polyamine transporter system (PTS) has been shown to allow polyamines and compounds that incorporate polyamines to enter cells.[21, 23, 24, 25] The PTS is expressed in high levels in cancer cells, such as those associated with the lung and the lymph nodes.[21, 23, 24, 25] Therefore, introducing compounds incorporated with polyamine chains might be able to target the cancer cells that express the PTS. Numerous research studies have attempted to optimize the composition of polyamines to stimulate cellular uptake; to date, there is no definite correlation between the polyamine composition and the cellular uptake rates.[21, 24, 25] In *E. coli*, it is found that there are specific transporters for two of the essential polyamines, putrescince and

spermidine. As such, incorporation of these polyamines into the drugs may provide a model of

drug-delivery.[26]

1.2 Polyamine anthracene conjugates

1.2.1 Design rationale

Polyamine anthracene conjugates, or Ants, are synthesized to be the target-specific agents

of cells expressing a high level of PTS (Figure 1). The Ants have the anthracene core with the

polyamine side chain(s) at the 9 or both the 9 and 10 positions. The design strategy aims to take

advantage of the PTS to deliver the toxin into cells. Many polyamine derivatives with different

PAH cores have been synthesized as molecular probes for DNA, proteins, and the polyamine

transporter system.[20, 22, 24, 27] The composition of the polyamine side chain of Ants is based on

putrescince and homospermidine; the design favors uptake via the polyamine transporter system.

	1: R = H (Ant N-Butyl) **2**: R = NH$_3$ (Ant4)
	3: R = H (Ant 44) **4**: R = CH$_3$ (Ant44NMe)
	5: R = H (44Ant44) **6**: R = CH$_3$ (MeN44Ant44NMe)
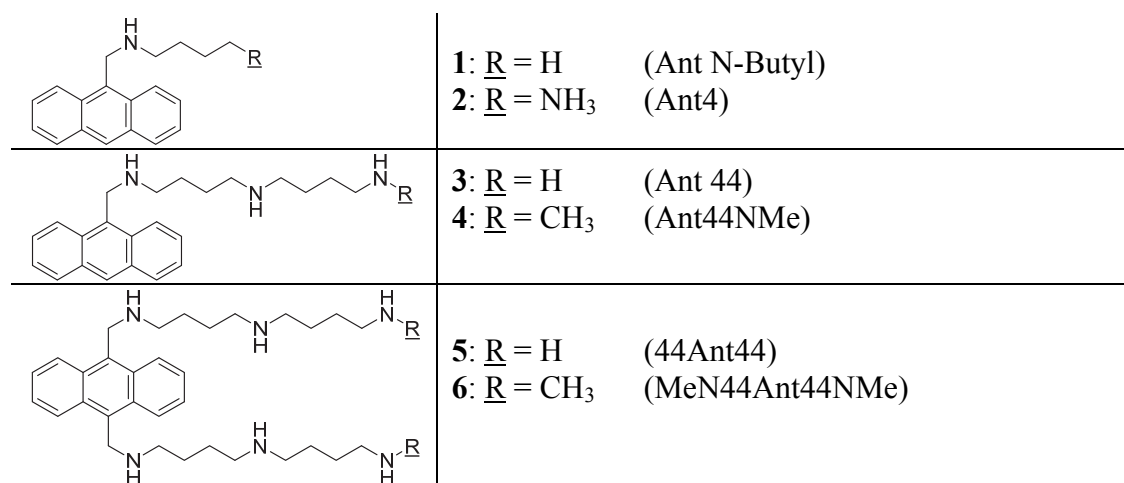
Figure 1. Polyamine anthracene conjugates **1 - 6**
Polyamine of **2** is a putrescince derivative
Polyamine of **3 - 6** are homospermidine derivatives
From reference [21] and [24]

1.2.2 Polyamine transporter system activity

Dr. Otto Phanstiel and his team at the University of Central Florida are investigating

cytotoxicity to ascertain if the PTS is utilized for cellular uptake of polyamine anthracene

conjugates (Ant). The selective uptake of the Ants by cancer cells would enhance their efficacy as anti-cancer agents. Cells can uptake Ants via the PTS, passive diffusion, and other alternative pathways. The Chinese hamster ovary (CHO) cells express a high level of the polyamine transporter system, similar to the cancer cells of the lung and lymph nodes; this characteristic makes CHO a good tool to study the delivery efficiency via cytotoxicity studies.[28] If the half maximal inhibitory concentration (IC_{50}) is low, the compound is highly cytotoxic. By comparing the cytotoxicity levels in a mutated cell line with suppressed PTS genes (CHO-MG) versus the wild type (CHO-WT), the PTS selectivity of the Ants can be determined. Currently, the cytotoxicity in the absence and presence of PTS is high for compounds under investigation with the exception of **6**. Compound **6** is not toxic in the absence of the PTS as shown in Table 1; however, the relatively small IC_{50} value signifies that the compound is extremely toxic in the presence of the PTS. The IC_{50} ratio of **6** is desirable due to the high possibility that the cytotoxicity is caused by PTS-assisted transport into the cell and subsequently intracellular interaction with macromolecules, a characteristic of the target-specific anti-cancer agent delivery design.[6] Further investigation by Phanstiel and co-workers suggests that polyamine oxidase is preventing the uptake of the Ants via PTS.[24] Polyamine oxidase metabolizes primary polyamine derivatives; once oxidized, the polyamine cannot be recognized by the PTS, leading to a similar cytotoxicity between the two cell lines. When aminoguanidine is used to inhibit the enzymes, the PTS system does not show selectivity between the two analogs (*i.e.*, **5** and **6**) as shown in Table 1. The difference between these two compounds is methylation converts the terminal primary amine to a secondary amine, which protects the polyamine derivatives against the polyamine oxidase and may improve the uptake via PTS. The PTS in the CHO-WT has a high selectivity for

di-substituted Ants **5** and **6** over the mono-substituted Ants in the presence of the inhibitor; without the inhibitor, the PTS only has high selectivity for the methylated **6**.[24]

Table 1. The cytotoxicity of the polyamine anthracene conjugates in the absence and presence of the polyamine transporter system (PTS) without and with polyamine oxidase inhibitor

Cmpd	Without inhibitor			With inhibitor		
	IC_{50} (no PTS) CHO-MG (µM)	IC_{50} (PTS) CHO-WT (µM)	Ratio	IC_{50} (no PTS) CHO-MG (µM)	IC_{50} (PTS) CHO-WT (µM)	Ratio
1	11.2 (± 2.3)	10.5 (± 2.0)	1.1	n.d.	n.d.	n.d.
2	7.6 (± 0.4)	7.7 (± 0.5)	1.0	n.d.	n.d.	n.d.
3	2.2 (± 0.1)	1.5 (± 0.02)	1.5	13.7 (± 1.3)	0.32 (± 0.01)	43
4	11.3 (± 2.2)	2.1 (± 0.06)	5.4	10.7 (± 1.2)	2.8 (± 0.2)	3.8
5	8.4 (± 0.7)	4.0 (± 0.03)	2.1	> 100	0.028 (± 0.001)	> 3571
6	> 100	0.084 (± 0.002)	> 1190	> 100	0.083 (± 0.004)	> 1204

CHO-MG: Chinese hamster ovary cell line - mutated suppressed PTS genes
CHO-WT: Chinese hamster ovary - wild type
n.d.: not determined
IC_{50}: half maximal inhibitory concentration
From reference [21] and [24]

$$Ratio = \frac{IC_{50}\ CHO\text{-}MG}{IC_{50}CHO\text{-}WT}$$

1.2.3 Possible intracellular interactions of polyamine anthracene conjugates

There are many intracellular interactions that cause cytotoxicity and cell death, such as the inhibition of a vital protein, production of cytotoxic metabolites, detrimental mutation, etc. Proteins and DNA are potential targets for the Ants because the polyamine side chains are derivatives of natural polyamine, such as putrescine, that has been shown to interact with these macromoelcules.[29] With respect to DNA, the positive charged polyamine side chain(s) can potentially alter the negatively charged phosphodiester backbone to separate adjacent DNA base pairs via electrostatic and H-bonding interaction, allowing the planar anthracene core to insert between the DNA base pairs better.[30, 31] The Ants can bind to DNA via either classical intercalation if Ants is mono-substituted, or in a threading intercalation mode if di-substituted.[32, 33] While the Ant can generate singlet oxygen and hydroxyl radicals upon irradiation with the UV light, the 9, 10 positions of the polyamine chains inhibit the oxidation of the anthracene core.

1.2.4   Ions in the eukaryotic nucleus

The nucleus contains various metals, such as Mg^{2+} and Na^+, that perform a variety of essential functions. [34, 35, 36] The divalent cation, Mg^{2+}, is critical in stabilizing the backbone of DNA due to its composition of phosphodiester anions.[36] The monovalent cations, Na^+ and K^+, also participate in the stabilization of DNA.[37, 38] Cation concentrations are varied across the different types of cells and the types of organism; however, in the nucleus, they are typically between 100 to 300 mM for each monovalent ion (Na^+ and K^+).[39, 35, 40] These monovalent ions can compete with the positive amine on the polyamine chain of the anthracene for the negative phosphodiester backbone, thereby decreasing the DNA binding affinity of the Ant.

1.2.5   Study of the interaction between DNA and polyamine anthracene conjugates under high ionic conditions

The purpose of the research described in this thesis is to determine if DNA is a potential target of the Ants in cells that express the PTS. The cations of the salts can interact with the negative phosphodiester backbone to stabilize the DNA structure further, and the chloride anion can have electrostatic interactions with the positive amino groups on the polyamine chains. Therefore, it is imperative to determine the interference effects of a high ionic strength environment on the DNA binding affinity of the Ants. The ionic conditions explored in this study are 10 mM sodium phosphate buffer (pH 7.0) in the absence (for the low salt environments) and presence of 150 mM NaCl and 260 mM KCl to represent the high salt condition in the cell nucleus.[30] The polyamine anthracene conjugates, as shown in Figure 1, were studied via UV-visible spectrophotometry analysis, circular dichroism and induced circular dichroism analysis, ethidium bromide displacement assay, and agarose gel shift assays to ascertain the degree of DNA binding interactions under low and high salt conditions.

2 EXPERIMENT

2.1 Materials and instruments

Agarose (A9539), sodium chloride (S9888), potassium chloride (P3911), sodium phosphate monobasic monohydrate (S9638), sodium phosphate dibasic (S5136), dimethyl sulfoxide (472301), were from Sigma-Aldrich. PUC19 plasmid DNA was cloned and quantified from XL-1 blue *E. coli* competent cells (Stratagene). UltraPure™ Calf Thymus DNA (CT-DNA) Solution, average size $\leq$ 2000 bp came from Life Technologies. Ethidium bromide (892829) was from GTI Laboratories Supplies. Polyamine-anthracene conjugates were synthesized by Dr. Jennifer Archer in the Phanstiel Group at the University of Central Florida, as shown in Figure 1.

A Shimadzu UV-2401 PC spectrophotometer, equipped with UVPC v3.9 software, was utilized to record UV-visible spectra. A Jasco J-810 Spectropolarimeter, with a J-800 control driver v1.27.00, was used to obtain circular dichroism (CD) and induced CD (ICD) spectra. Fluorescence data were acquired via Corning™ polystyrene white 96-well assay microplates and a *FLUO*star 4.31-0 microplate reader.

2.2 Methods

2.2.1 General

One M solutions of dibasic (pH 7.0) and monobasic sodium phosphate were prepared in ddH$_2$O to make 100 mM sodium phosphate buffer (pH 7.0). The 1 M NaCl and 1 M KCl solutions were made with ddH$_2$O for the high salt conditions. The calf thymus DNA (CT-DNA) concentration of the original stock was ascertained again via DNA quantitation by UV-visible spectrophotometry using an average extinction coefficient of 50 µg/mL. A 10,000 µM bp CT-DNA solution was diluted from the original stock solution with the 100 mM sodium phosphate

buffer (pH = 7.0); a 5,000 µM bp CT-DNA solution was made by diluting of the 10,000 µM stock with 100 mM sodium phosphate buffer and ddH$_2$O. The final buffer concentration was ~5 mM for 10,000 µM stock and ~25 mM for 5,000 µM stock. All stocks of Ants were made at high concentration (10 mM) in dehydrated DMSO and were stored at -20°C. The Ants, **4**, **5** and **6**, were the exceptions due to scarcity; their concentrations in DMSO were 2.10, 3.92 and 2.20 mM, respectively. Before the UV-visible titration, the original stock of Ant was diluted to 500 µM with ddH$_2$O, and the sub-stock was stored in the freezer. For the **5** and **6**, the stocks had to be heated at 37°C for 7 min before diluting with ddH$_2$O to make the sub-stock. A 5.088 mg/mL ethidium bromide solution was prepared in ddH$_2$O. All experiments were conducted at room temperature and pH 7.0.

2.2.2   Circular dichroism

Four samples containing 10 mM sodium phosphate buffer (pH 7.0), 150 µM bp CT-DNA in 10 mM sodium phosphate buffer (pH 7.0), 50 µM Ant in 10 mM sodium phosphate buffer (pH 7.0), and 150 µM bp CT-DNA + 50 µM Ant in 10 mM sodium phosphate (pH 7.0), were made for the low salt CD experiment. For the high salt conditions, 150 mM NaCl and 260 mM KCl were added to in each sample. The induced CD spectra were obtained from 450 to 300 nm in a 1 cm, 3 mL quartz cuvette. The CD spectra were recorded from 300 to 200 nm in a 0.2 cm, 1 mL quartz cuvette. The program was set up to run at 100 nm/min with a 2 s response time, a 1 nm slit, and over 12 acquisitions. The sensitivity was high (5 mdeg) from 450 nm to 300 nm and standard (100 mdeg) from 300 nm to 200 nm. The experiment was performed once.

2.2.3   DNA binding affinity of the ethidium bromide

The assay employed was adapted from the literature and was done in triplicate.[41] A series of 21 samples was made: a 1700 mL standard solution for EtBr, and 1700 mL stocks with 0.25

increasing per $\log_{10}$ concentration of the CT-DNA in molarity (*i.e.*, log [DNA, M] from -8 to -3.25). Each stock was divided into three 500 μL aliquots; 1 μL of 5.088 mg/mL was then added to each aliquot ([EtBr]$_{final}$ = 12.9 μM) for UV-visible spectrophotometry, scanning from 200 nm to 700 nm. The DNA binding affinity of the ethidium bromide (K_e) was ascertained using the non-linear least squares method according to the following equations from reference [41]:

$$A = \varepsilon_o(C_t - C_b) + \varepsilon_b C_b \qquad (1)$$

$$KC_b^2 - C_b(KD_t + KC_t + 1) + KD_tC_t = 0 \qquad (2)$$

where A is the absorbance at each DNA concentration, ε_0 is the molar extinction coefficient of the free ligand, the ε_b is the molar extinction coefficient of the DNA bound ligand, C_t is the total ligand concentration, C_b is the bound ligand concentration (equation 2 was solved for C_b by the quadratic formula), D_t is the total DNA concentration, and K is the DNA association constant.[41]

Equation 2 was converted to the quadratic formula and incorporated into equation 1; the completed equation was converted in a readable equation into Igor: C_t is constant1, while K, ε_b, and ε_o are m4, m3, and m2, respectively. The parameter, m2, was locked within 5% error of the real ε_o value. The m3 was locked above 1000 M^{-1} cm^{-1}. The m4 was allowed to float. The comparison between the predicted ε_b and ε_o and the real values is shown in Table B1 in the Appendix B.

2.2.4   *Ascertaining DNA binding affinity of Ants via UV-visible titration*

UV-visible titrations were recorded under two different conditions, low salt (10 mM sodium phosphate buffer, pH 7.0) and high salt (10 mM sodium phosphate with 150 mM NaCl and 260 mM KCl). The 5,000 μM bp CT-DNA stocks were used for the low salt experiments, and 10,000 μM bp CT-DNA stocks for the high salt experiments. For reference, the

concentration of each conjugate was shown in Table 2. CT-DNA was added to fixed concentrations of Ants in increments of 0.5 to 2 µL until no changes in absorbance could be observed, an indication that the Ant was bound entirely to DNA. The spectra were adjusted for dilution resulting from the DNA addition. The DNA binding constant (K_b) was determined with the equations 1 and 2 using the absorbance at 387 nm for the mono-substituted Ants (**1 - 4**) and 394 nm for the di-substituted (**5** and **6**); the monitored absorbances at these wavelengths represented the binding of [Ants] to form Ant-DNA complex. The experiment was done in triplicate except for **5** under low salt condition; this experiment was performed twice.

2.2.5 Ethidium bromide displacement via fluorescence microplate assay

The ethidium bromide (EtBr) and CT-DNA stock solutions with molar ratios of 1.26:1 (63 µM EtBr for **5** and **6**, 31.5 µM EtBr for **3** and **4**, and 15.75 µM EtBr for **1** and **2**) were prepared and equilibrated for 30 min in the dark for the low salt conditions. For the high salt experiments, 15.75 µM EtBr and 75 µM bp DNA (0.21:1 ratio) were employed. The set up of the microplate involved a triplicate of blanks (10 mM sodium phosphate buffer, pH 7.0), a triplicate of the EtBr + DNA stocks, and a triplicate of samples with increasing concentrations of the Ant (the range was adjusted based on the preliminary data). A total of 20 µL of the EtBr + CT-DNA solution was added to all sample wells except for the blank; the final volume of each well was 100 µL. The final concentrations in the low salt experiment were as followed: a molar ratio of 1.26 EtBr to 1 DNA bp (Table 2), and 10 mM sodium phosphate buffer (pH 7.0); for the high salt experiments, 3.15 µM EtBr and 15 µM bp CT-DNA were used with 150 mM NaCl and 260 KCl (Table 2). The excitation wavelength was 540 nm, and the emission wavelength was 590 nm. The instrument scans the microplates four times with five flashes per scan per well. The apparent binding affinity of the Ant was calculated using equation 3:

$$K_{app} = K_e \times \frac{[EtBr]}{[Ant]_{50}} \quad (3)$$

where K_{app} is the apparent DNA binding affinity, [EtBr] is the concentration of the ethidium bromide, K_e is DNA binding affinity of EtBr, and $[Ant]_{50}$ is the concentration of the Ant at 50% EtBr-DNA fluorescence emission intensity.

2.2.6 Discerning the effects of the Ants on DNA migration via gel shift assay

The 1.5% gel was made with 1.5 g agarose in 100 µL of 1X TAE buffer for a typical small gel box. The electrophoresis box was filled with 1X TAE buffer. Samples contained 10 mM sodium phosphate buffer (pH 7.0), 30 µM bp pUC19 DNA, and the Ant (40 µL total

volume). After a 30 min equilibrate period, 3 µL of the loading buffer was added to each sample before loading in the wells of the gel. The gel was run for 1.75 h at 80 V. After the run, the gel and half the 1X TAE running buffer were transferred to a container. A total of 200 µL of ethidium bromide dye (5 mg/mL) was then added, and the gel was equilibrated in the EtBr solution for 30 min.

3   RESULTS and DISCUSSION

The aim of this study was to investigate the structural influence of the number of the amino groups and the number of polyamine side chains on polyamine anthracene conjugate - DNA interactions. The Ants have been studied extensively with respect to cytotoxicity, spectroscopy properties, and DNA interactions.[20, 22, 42, 43] The polyamine side chains, owning to their protonation potential, are expected to further enhance the DNA binding affinity of the anthracene, a well-known DNA intercalator. The more positive amino groups there are, the higher the expected DNA binding affinity.

3.1   DNA unwinding by polyamine anthracene conjugates

Compounds that bind to DNA via intercalation unwind the DNA helix. The CD spectra of the DNA are the same under both low salt and high salt conditions, which indicates that the high salt conditions do not change the DNA conformation significantly (Figure 2). However, upon addition of the Ant **1 - 4** and **6**, the DNA unwinding by the Ants binding caused a decrease in the DNA CD signal in the 280 nm - 300 nm region as shown in Figure 2.[44] Furthermore, the apparent degree of unwinding followed the order, **6** > **4** > **3** > **2** > **1**, which reflects the number of positive cations of the ligand. While the DNA unwinding was significantly lower under the high salt condition, the order of unwinding was the same (Figure 2B). Ant **6** is di-substituted with two trivalent polyamine side chains, which creates a more robust DNA unwinding signal. Ant **4** has a

slightly higher DNA unwinding than Ant **3**; the data suggest the transformation from a primary to a secondary amine increases the protonation potential, thereby increasing the DNA unwinding. An explanation for this occurrence is that a conversion of a primary amine to a secondary amine via methylation may increase the pK_a slightly.[45]

Although the Ants are not chiral at room temperature, they can form chiral complex with DNA upon interaction.[44] The formation of the chiral complex generates an induced CD (ICD) signal as shown in Figure 2B and 2D. The pattern of the ICD signals matches the pattern of the UV-visible absorption spectrum at the DNA saturation point of the Ants (Figure A1 to A5 in Appendix A). The DNA unwinding and the ICD signal pattern together suggest that the DNA interaction of Ants involves intercalation.[44] The CD and ICD spectra both indicate that the addition of salts reduces DNA binding affinity of the Ants. The degree of apparent helical unwinding and the ICD signals are reduced in intensity. Notwithstanding, under the high ionic strength conditions, compound **6** shows evidence of robust DNA interactions. The cationic di-substituted Ants with trivalent polyamines can interact with two parts of the anionic phosphodiester backbone of the nucleic acids.

Regarding the level of electrostatic and intercalation, there may be differences based on the composition of the polyamine. For Ants, the distance between the anthracene and the polyamine side chains are short; therefore, the polyamine side chain(s) can surround the anthracene core. While **1** shows little to no unwinding as shown in Figure 2, the ICD signals suggest intercalation. Thus, the polyamine plays a small role in the interaction between **1** and DNA, and the level of intercalation is higher than electrostatic binding. For the di-substituted Ant **6**, the trivalent polyamine side chains can inhibit intercalation due to electrostatic repulsion if the salt concentrations surrounding the phosphodiester backbone of nucleic acids are high enough. In

the case of high salt conditions, the trivalent polyamine side chains of **6** are able to overcome the high ionic strength, relaxing the DNA conformation to allow space for intercalation. Overall, the relative levels of intercalation and electrostatic are dependent based on the structure of the Ants and the ionic environment of DNA.
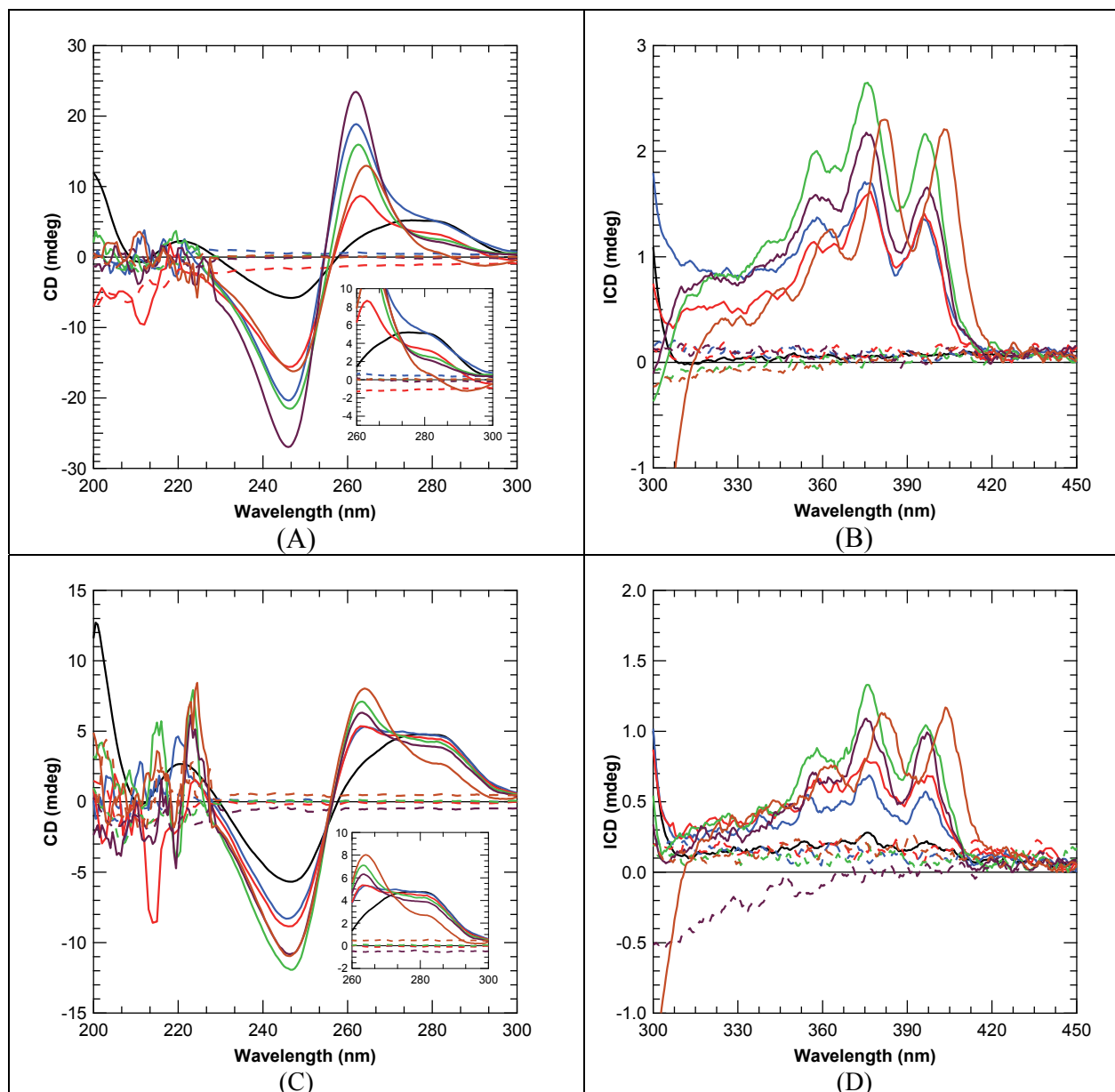
Figure 2. CD and ICD spectra of 1-4, 6

Circular dichroism and induced circular dichroism of 50 µM of Ant and/or 150 µM of CT-DNA in 10 mM sodium phosphate buffer (pH 7.0) in the absence (A and B) and presence (C and D) of 150 mM NaCl and 260 mM KCl. Inset: CD spectra from 260 nm to 300 nm. Appendix A shows CD, ICD, and the matching UV-visible spectra of each Ant.

DNA — 1 — 2 — 3 — 4 — 6
1 + DNA — 2 + DNA — 3 + DNA — 4 + DNA — 6 + DNA

3.2 DNA binding affinity of ethidium bromide

Ethidium bromide is a known intercalator of DNA. To perform an ethidium bromide displacement assay, it is necessary to study the EtBr-DNA interactions under low salt and high salt conditions. The UV-visible spectra of the increasing DNA concentrations exhibit a hypochromicity and red shifting in EtBr absorption (Figure 3). For the low salt experiment, the 515 nm point is pseudo isosbestic, which indicates another product is formed, potentially base stacking of the ethidium bromide. For the purpose of the analysis, the 515 nm point is assumed to be isosbestic. The hypochromic shift at 480 nm under the high salt conditions (Figure 3B) has slower onset compared to the low salt (Figure 3A), which indicates the high salt impedes the interaction between ethidium bromide and DNA. The absorbance at 480 nm was recorded to monitor the disappearance of ligand (EtBr) and to calculate the binding constant using equations 1 and 2.
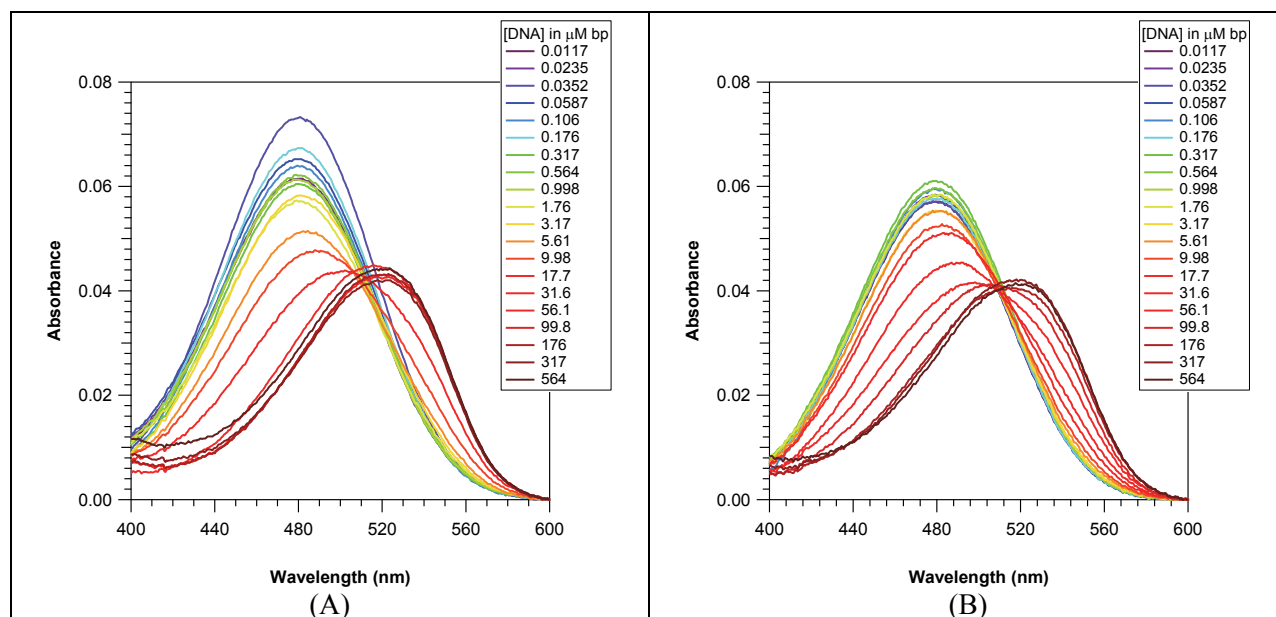
Figure 3. UV-visible titration of EtBr with increasing DNA concentrations
12.9 μM of EtBr was titrated with increasing DNA concentration under 10 mM sodium phosphate buffer (pH 7.0) in the absence (A) and presence (B) of 150 mM NaCl and 260 mM KCl. The spectra exhibit a hypochromicity and red shifting as more DNA is added. The UV-visible spectra have an isosbestic point at 515 nm, which indicates free and DNA bound forms of EtBr.

The spectra in Figure 3 show that the nature of the solution conditions changes the DNA binding constants. Thus, it is necessary to determine the exact DNA binding affinity of the ethidium bromide (K_e) under the low salt and the high salt conditions. Furthermore, it is important to utilize the corrected K_e under different salt conditions for the equation 3 in the ethidium bromide displacement assays (Figure 4). The K_e was calculated by converting the equations 1 and 2 into a computing equation in the curve fitting tool of Igor 6.34 (method section). Determination of the DNA binding constant of ethidium bromide by Garbett and co-workers showed the K_e equals to $1.23 \pm 0.07 \times 10^5$ M^{-1}.[46] This value was lower compared to the $K_e^{\text{low salt}} = 3.68 \pm 0.14 \times 10^5$ M^{-1} value obtained using equations 1 and 2 (Figure 4A). The buffer solution used by Garbett and for this experiment is similar (10 mM sodium phosphate buffer, pH 7.0), except for an additional 100 mM NaCl in the buffer for Garbett's experiments; this suggests the high salt concentration decreases the DNA affinity of the EtBr. Therefore, the $K_e^{\text{low salt}}$ from the UV-visible titration data (Figure 4A) is within a reasonable range of the reported value. Data analysis shows $K_e^{\text{high salt}}$ is $2.95 \pm 0.08 \times 10^4$ M^{-1} under the high salt condition (Figure 4B). The 12-fold decrease in binding constant indicates that increasing the concentration of positive cations alters the DNA binding constant of EtBr considerably. The ethidium binding constants, $3.68 \pm 0.14 \times 10^5$ M^{-1} for the low salt, and $2.95 \pm 0.08 \times 10^4$ M^{-1} for the high salt condition calculated in this work, were utilized for the determination of the apparent binding constant of Ants via EtBr displacement. The ε_0 and ε_b under low salt condition are 4999 ± 80 and 2226 ± 96 M^{-1} cm^{-1}; they are 4611 ± 52 and 1983 ± 72 M^{-1} cm^{-1} for the high salt conditions, respectively. These values are lower than the literature values, 5560 ± 81 and 1837 ± 79 M^{-1} cm^{-1} (unknown ionic strength conditions), respectively.[41] The differences may be the results of the low and high ionic conditions.
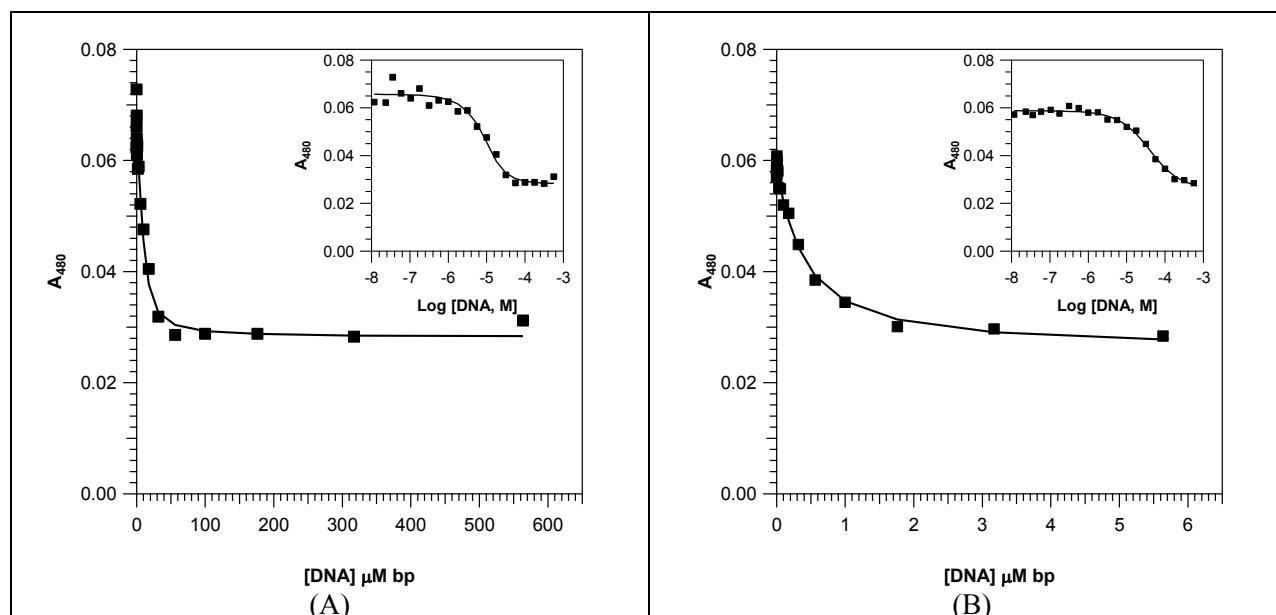
Figure 4. Xiaogang analysis of DNA binding constant via the UV-visible titration of EtBr with DNA

Absorbance at 480 nm of 12.9 μM of EtBr was titrated against with increasing DNA concentration under 10 mM sodium phosphate buffer (pH 7.0) in the absence (A) and presence (B) of 150 mM NaCl and 260 mM KCl. The model (solid line) is fitted onto the data (diamond) via non-linear least squares method with equation 3. Pearson's $R > 0.9700$. Inset: absorbance at 480 nm as a function of the $\log_{10}$ [DNA, M] for better visualization.

3.3 UV-visible spectral analysis and DNA binding constant determination of the Ants

The spectra of the mono-substituted and the di-substituted Ants have a slight difference: the peak at 387 nm for the mono shifts to 394 nm for the di-substituted as shown in Figure B1 in Appendix B2. The second substituted polyamine side chain may have caused the shift. To determine DNA binding constants, increasing concentration of DNA were added to fixed concentrations of the Ants and UV-visible spectra were recorded after each DNA addition. As the concentration of DNA increases, the UV-visible spectra display hypochromic and red shifting as illustrated in Figure 5. There is an isosbestic point at 392 nm for the mono-substituted Ants (**1** to **4**), and at 398 nm for di-substituted **5** and **6**. The isosbestic point indicates at least a free and bound form of the Ants, and the hypochromic and red shifting indicate possible intercalation. Similar DNA-induced absorbance changes have been observed in other types of polyamine anthracene conjugates studied by Rodger, Kumar, and Wilson.[20, 44, 47] The high salt

titration requires a significantly higher DNA concentrations relative to the low salt conditions; however, this causes the UV-visible spectral baseline to shift in the 420 nm - 450 nm region when making the adjustment for sample dilution upon DNA addition (Figure 5). The patterns described here apply to the other five Ants, with the exception of Ant **5**, as shown in Figure B1 in Appendix B2. As mentioned above, the UV-visible spectra of Ant **5** display high baseline shifts when DNA is added under the low salt condition, which may be caused by aggregation of Ant (Figure B1).
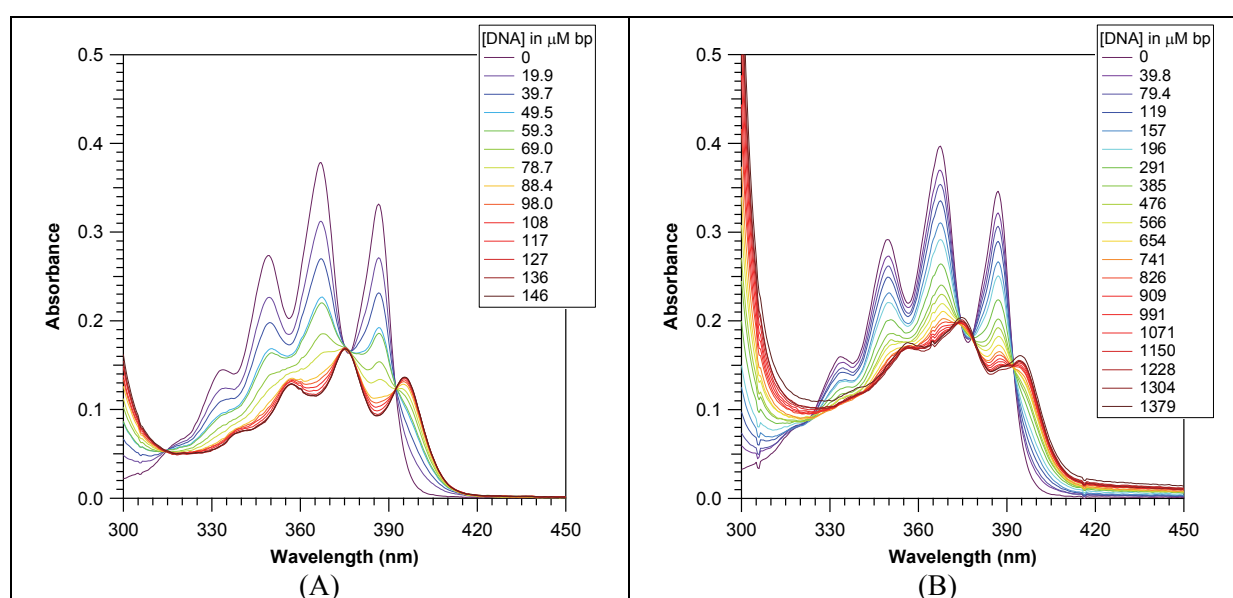
Figure 5. Representative UV-visible titration (**2**)

85 µM of Ant **2** is titrated with increasing DNA concentrations in 10 mM sodium phosphate buffer (pH 7.0) in the absence (A) and presence (B) of 150 mM NaCl and 260 mM KCl. The spectra exhibit hypochromic and red shifting as more DNA is added. The shift is slower under the high salt condition compared to low salt. The isosbestic point at 392 nm indicates a free and DNA bound form of **2**. Adjustment for sample dilution causes artificial baseline shifting in the 420 - 450 nm region under the high salt conditions. Appendix B2 contains the representative UV-visible titration spectra of the other Ants.

Due to light scattering observed for Ant **5** under the low salt condition, the $K_b^{\text{low salt}}$ of Ant **5** was not calculated (Figure B1 in the Appendix). There are also concerns regarding the final volume being significantly higher than the original 500 µL volume in the cuvette prior to DNA addition, especially for the weak binding Ants under the high salt conditions (*e.g.*, 625, and 555 µL for Ant **1** to **3**, respectively); when the volume is adjusted for the sample dilution, the absorbance can shift upward if the dilution ratio is too high, which results in artificial baseline

shift at 420 to 450 nm as shown in Figure 5 and Figure B2. The binding constants under the high

salt conditions may be adversely affected by this adjustment. The K_b were determined for the

absorbance at 387 nm for the mono-substituted and 394 nm for the di-substituted Ants using

equations 1 and 2 to determine binding constants (K_b). The K_b was calculated by converting the

equations 1 and 2 into a computing equation in the curve fitting tool of Igor 6.34 (method

section), and manually adjusting the given results for the analysis of variance to produce a

Pearson's R (least square curve fits) value close to 1; an example is Ant **2** as shown in Figure 6.

The plotting for each UV-visible spectra is in Figure B3 and B4 in Appendix B3.
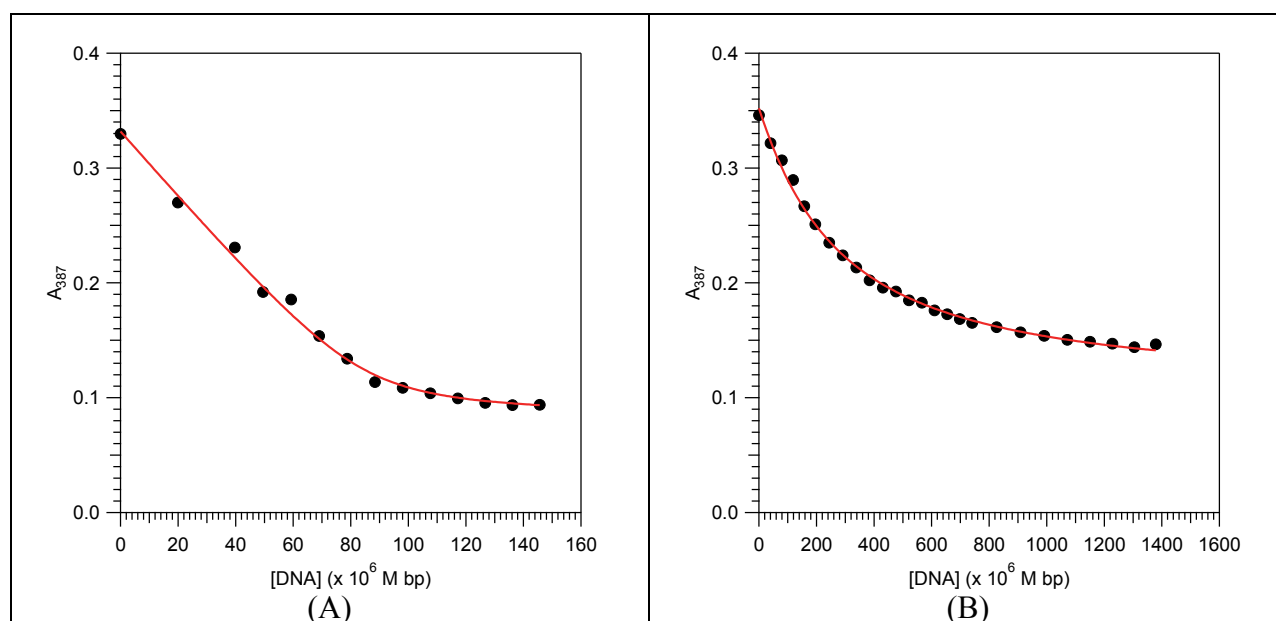
Figure 6. The Xiaogang DNA binding constant analysis (**2**)
Xiaogang analysis of (A) Figure 5A and (B) Figure 5B. The model (solid) is fitted onto the data (circle) via equations 1 and 2 with non-linear curve squared analysis. Pearson's R value: (A) 0.9976, (B) 0.9988. Xiaogang analysis of all of the Ants is in Figure B3 and B4 in Appendix B3

The high salt conditions significantly decrease the K_b; the two salt conditions result in

different orderings of binding constant. From highest to lowest, the order of $K_b^{\text{low salt}}$ is **2** > **4** > **3**

$\approx$ **6** > **1**, and the $K_b^{\text{high salt}}$ is **6** > **5** > **4** $\approx$ **3** $\approx$ **2** > **1**. Closer analysis of the Xiaogang model reveals

that, while the curve fitting analysis show good to excellent fits (Pearson's R > 0.9700), the

model does not fit all the data point under the low salt and high salt condition for Ants **3** and **4**

(Figure B3 and B4). The extinction coefficient of the DNA bound (ε_b) obtained from the equation 1 does not match with the real value (Table B1 in the Appendix B4). While there is no correlation between the structure and the binding constant in the UV-visible titration data, the analysis agrees with the other experiments that the Ant **1** has the weakest DNA interaction among the six polyamine anthracene conjugates and that Ants are strong DNA binders under both low and high salt conditions.

An empirical observation of the UV-visible spectra and their hypochromic shift data give some hints relating to the relative DNA binding affinities of the Ants (Table 2). By comparing the hypochromic shift of the free Ants to the saturation point where all of the Ants are DNA bound (Figure B3 and B4), the order of decreasing DNA binding affinities is as follows: **6** > **5** > **4** ≈ **3** ≈ **2** > **1** under low salt conditions, and **6** > **5** > **3** > **4** ≈ **2** > **1** under high salt conditions (Table 2). These observations are relatively consistent with the data obtained in circular dichroism experiments. An indirect method, ethidium bromide displacement, was also used to determine the apparent binding constant of Ants.

Table 2. The DNA binding affinities of the polyamine anthracene conjugates via EtBr displacement and UV-visible titration analyses

Ant	EtBr Displacement Assay				UV-visible Titration[a]				
	[EtBr] (μM)	$K_{app}^{low\ salt}$ (x 10^4 M^{-1})	[EtBr] (μM)	$K_{app}^{high\ salt}$ (x 10^4 M^{-1})	[Ant] (μM)	Hypochromic % at λ_{max}	$K_b^{low\ salt}$ (x 10^4 M^{-1})	Hypochromic % at λ_{max}	$K_b^{high\ salt}$ (x 10^4 M^{-1})
1	3.15	0.88 ± 0.06	3.15	0.037 ± 0.001	48	31.1 ± 0.4	2.8 ± 0.3	$46 \pm 1^{\beta}$	$0.27 \pm 0.04^{\beta}$
2	3.15	29.7 ± 3.0	3.15	0.051 ± 0.002	85	28.4 ± 0.5	31 ± 2	$40 \pm 2^{\beta}$	$0.45 \pm 0.10^{\beta}$
3	6.3	151 ± 13	3.15	0.115 ± 0.006	54	27.7 ± 0.2	6.4 ± 0.6	$37 \pm 1^{\beta}$	$0.41 \pm 0.05^{\beta}$
4	6.3	201 ± 3	3.15	0.200 ± 0.004	48	28.8 ± 0.9	11 ± 1	40.8 ± 0.9	0.37 ± 0.04
5	12.6	276 ± 12	3.15	0.134 ± 0.005	60	$24.4 \pm 0.4^{\gamma}$	n.d.$^{+}$	31.1 ± 0.3	0.936 ± 0.012
6	12.6	447 ± 19	3.15	0.221 ± 0.009	50	22.4 ± 0.1	6.3 ± 0.3	30 ± 1	0.98 ± 0.03

n = 3 $^{\gamma}$n=2   n.d.: not determined $^{\beta}$Artificial baseline shift ^{a}Need to be revised $^{+}$High baseline shift
[EtBr]: the final concentration of EtBr in the sample   [Ant]: the concentration of Ant used in UV-visible titration
The ε_0 and ε_f for UV-visible Titration are in Table B1 in the Appendix B4
λ_{max} for **1** to **4** = 387 nm λ_{max} for **5** and **6** = 394 nm
$K_{app} = K_e \times \frac{[EtBr]}{[Ant]_{50}}$; ratio of EtBr:DNA = 1.26:1, $K_e^{low\ salt} = 3.68 \pm 0.14 \times 10^5$ M^{-1}
ratio of EtBr:DNA = 0.21:1, $K_e^{high\ salt} = 2.95 \pm 0.08 \times 10^4$ M^{-1}

3.4   Apparent DNA binding affinities of the polyamine anthracene conjugates

The ethidium bromide (EtBr) displacement assay can be used to give a good picture concerning the relative DNA binding affinities of closely related compounds. Because Ants are intercalators, they can theoretically displace the EtBr from DNA base pairs. The loss of the EtBr from the DNA helix quenches its fluorescence in the EtBr displacement assays. Increasing concentration of the Ants were added to solution containing DNA-bound EtBr. All of the Ants quenched EtBr fluorescence as shown in Figure 7. From the data, the concentration of Ants at 50% fluorescence intensity (C$_{50}$) was used to calculate the apparent binding constant, K_{app}, with equation 3. The low salt titration in Figure 7A shows four compounds (**3** to **6**) to have a ratio of Ant to EtBr less than 1, which implies that these Ants have a stronger DNA affinity than EtBr. However, the high salt conditions significantly impede DNA binding of EtBr, resulting in the ratio 1.26 EtBr:DNA used in Figure 7A not working well in forming the EtBr-DNA complex. The ratio 0.21 EtBr to DNA has shown similar fluorescence intensity under high salt when

compared to the ratio 1.26 under low salt condition, which implies the ratio is applicable for the EtBr displacement under high salt. Nevertheless, because the DNA concentration is higher than the concentration of the EtBr in the high ionic strength experiments, Ants can potentially bind to the DNA first before displacing the EtBr.
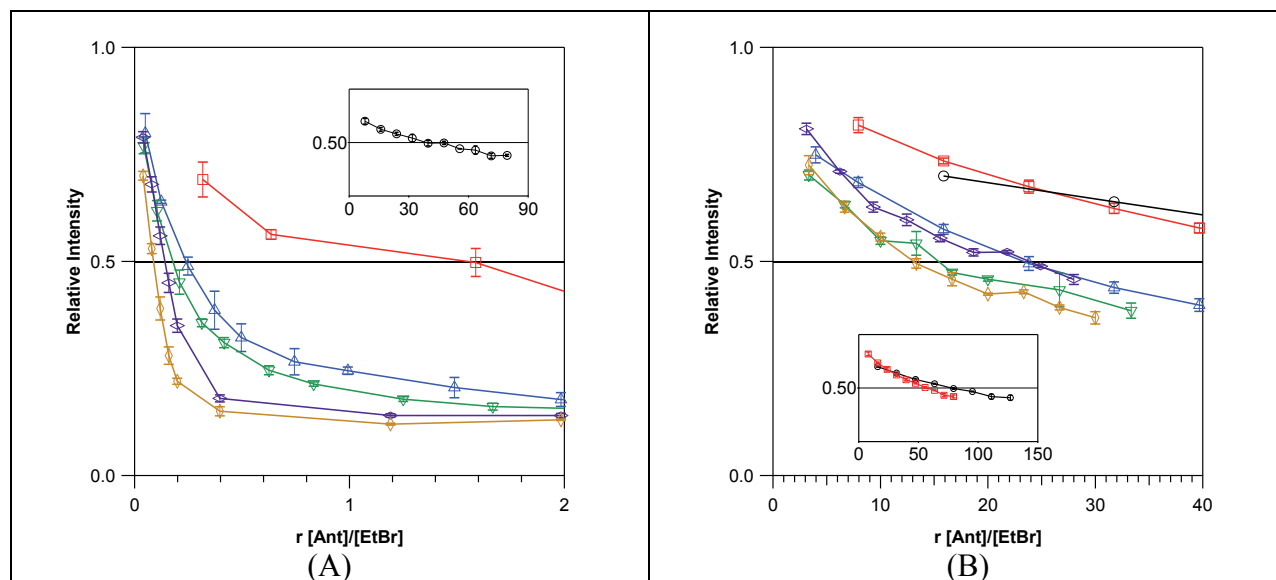
Figure 7. EtBr displacement of Ants **1** to **6**
The [EtBr] (Table 2) is titrated with increasing [Ants] in 10 mM sodium phosphate buffer (pH 7.0) in the absence (A) and presence (B) of 150 mM NaCl and 260 mM KCl. Excitation: 540 nm, emission: 590 nm. As the concentration of Ants increases, the EtBr-DNA emission decreases. Inset: relative fluorescence of **1** under low salt and **1** and **2** under high salt condition. ⊖ **1** ⊟ **2** △ **3** ▽ **4** ◇ **5** ◇ **6**

Although the EtBr displacements in Figure 7B display close associations to each other for Ant **3 - 6**, the determined C_{50} values and the following calculated K_{app} value have significant differences based on the standard deviation (Table 2). The apparent binding constants under the low salt conditions ($K_{app}^{low\ salt}$) have a direct correlation to the number of the amino groups and the length of the polyamine chain as follows: **6** >> **5** >> **4** >> **3** >> **2** >> **1**. In this experiment, Ant **6** to **3** have a higher apparent DNA binding affinity than the DNA binding affinity of the EtBr (446.6, 275.5, 200.6, 151.0, and 36.8 $\times 10^4$ M^{-1}, respectively, Table 2). The apparent binding constants of **1** and **2** are lower than EtBr under the low salt condition (Table 2). Furthermore, the $K_b^{low\ salt}$ of **2** is within range of the $K_{app}^{low\ salt}$ (31 v. 29.7 x10^4 M^{-1}, Table 2). The

comparison between the two binding constants data and the good fit of the Xiaogang model on the data suggest the $K_b^{\text{low salt}}$ of **1** and **2** are reliable. Ants **6** and **5** are stronger DNA binders than the other Ants most likely because they are di-substituted with trivalent polyamines compared to the mono-substituted Ants. The binding data suggest that methylation at the terminal amine(s) (**3** to **4** and **5** to **6**) enhances the DNA binding affinities, possibly due to increasing the protonation potential of the amino groups.[45]

As expected, the $K_{\text{app}}^{\text{high salt}}$ values were substantially lower compared to the $K_{\text{app}}^{\text{low salt}}$; although, the difference between each apparent binding constant was not as significant. The order of the Ants has slightly changed under the high ionic strength conditions (**6** > **4** > **5** > **3** > **2** > **1**), and none of the Ants has a higher apparent binding constant than EtBr. The change may be due to the Ants binding to DNA before displacing the EtBr. Thus, the $K_{\text{app}}^{\text{high salt}}$ is treated as a representative binding constant for comparison between the Ants under low salt and high salt conditions. Overall, **6** has the strongest apparent DNA binding constant in the Ant series.

3.5 The effect of Ants on the migration of DNA bands in agarose gels

In gel electrophoresis, the DNA bands move from the negative cathode to the positive anode due to the anionic phosphodiester backbone of the nucleic acid. The rate of migration of the DNA band is directly correlated to the molecular weight (or size) and the DNA conformation. Complex formation between DNA and positively charged ligands leads to higher molecular weights, reduced negative charge, and possible DNA conformational changes that can change the migration of the DNA bands. As shown in Figure 8, Figure 9, and Figure 10, the relative mobilities of the complexes formed between plasmid DNA and the Ants ranked, from slowest to fastest migration under dark conditions, is as follows: **6** > **5** > **4** ≈ **3** > **2** > **1**. There is no significant shift between Ant **1** and the reference DNA band (without Ant) despite the high

ratio of Ant to DNA (10:1) as shown in Figure 8. The high salt conditions are not usually used

the gel shift assays because the salts can disperse from the wells of the gel. Therefore, low salt

and high salt conditions produced generally nearly identical results. Overall, the di-substituted

Ant **6** has the strongest ability to alter the mobility of plasmid DNA. The methylation at the

terminal amine of Ant **6** may have contributed to its ability to retard DNA migration more

efficiently compared to Ant **5.**

Lane	1	2	3	4	5	6	7
[Ant] (µM)	0	50	150	300	10	50	100
Legend	DNA		**1**			**2**	
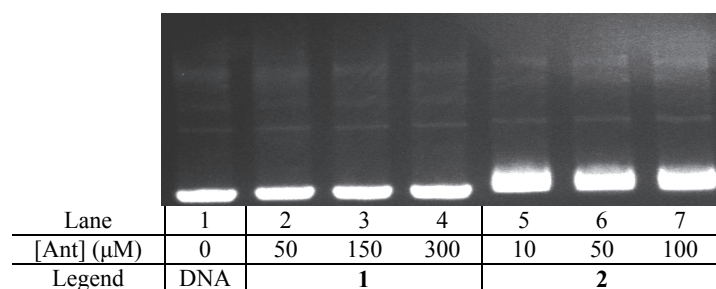
Figure 8. Effect of increasing concentrations of **1** and **2** on the relative gel mobilities of DNA
30 µM bp of pUC19 DNA is titrated with increasing [Ant] under the low salt (10 mM sodium phosphate buffer, pH 7.0)
conditions for 1.75 h at 80 V.

Lane	1	2	3	4	5	6	7
[Ant] (µM)	0	0.5	2.5	5.0	0.5	2.5	5.0
Legend	DNA		**3**			**4**	
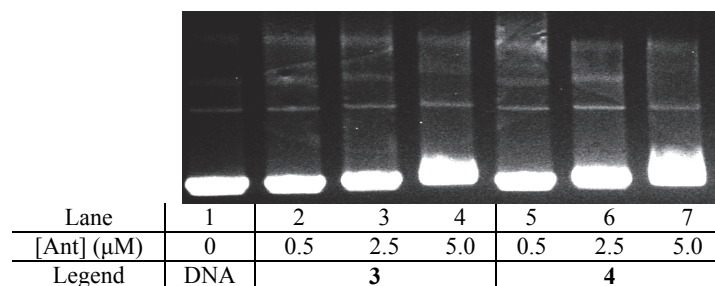
Figure 9. Effect of increasing concentrations of **3** and **4** on the relative gel mobilities of DNA
30 µM bp of pUC19 DNA is titrated with increasing [Ant] under the low salt (10 mM sodium phosphate buffer, pH 7.0)
conditions for 1.75 h at 80 V.

Lane	1	2	3	4	5	6	7
[Ant] (µM)	0	0.5	2.5	5.0	0.5	2.5	5.0
Legend	DNA		**5**			**6**	
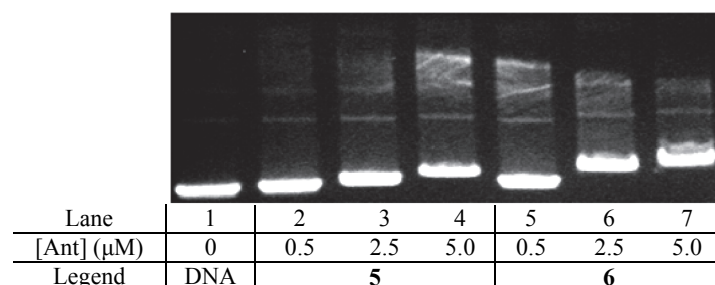
Figure 10. Effect of increasing concentrations of **5** and **6** on the relative gel mobilities of DNA
30 µM bp of pUC19 DNA is titrated with increasing [Ant] under the low salt (10 mM sodium phosphate buffer, pH 7.0)
conditions for 1.75 h at 80 V.

4   CONCLUSIONS

The polyamine anthracene conjugates described in this thesis incorporated known polyamines that cells uptake actively via the polyamine transporter system. The composition of the Ants included structural features that enhance DNA interactions: the polycyclic aromatic hydrocarbon anthracene core can intercalate between the DNA base pairs, and the cationic polyamines can interact electrostatically with the anionic phosphodiester backbone of nucleic acids under physiological conditions. This thesis focuses on investigating the correlation between the composition of the polyamine side chain(s) and the DNA binding affinities of Ants. The overwhelming majority of data reported here have pointed to Ant **6,** MeN44A44NMe, as having the strongest DNA binding affinity (Table 3). If the order obtained from the empirical observation of the hypochromic effect of the UV-visible spectra at the saturation points of the Ants is considered instead of the DNA binding constant, the ordering would be similar to the ordering of the other experiments. The high ionic strength conditions significantly hinder the DNA binding affinity of the Ants, which is expected considering the significant differences between the concentration of salts (NaCl and KCl) compared to the concentration of the Ants. There is a general trend in which increasing positive amino groups increase DNA binding as observed in circular dichroism, EtBr displacement, and gel shift assays. The di-substituted Ants have relatively higher DNA binding affinities than the mono-substituted Ants. The monovalent cations Na(I) and K(I) can stabilize the DNA structure, and the chloride ions can interact with the positive amino groups of the polyamines. Considering the cytotoxicity of the Ants in cell lines that express the PTS, it is probable that the compounds, or their by-products, have intracellular interactions with different macromolecules within the cells. However, on analysis of

the Ants studied in this thesis suggests that the di-substituted Ant **6** has the highest potential to

interact with DNA after taking advantage of the PTS to enter cells.

Table 3. Ranking of the DNA interactions of the Ants

Experiment	Condition	Strongest to weakest					
Cytotoxicity study:	Normal	**6** >>> **4** >	**5** >	**3** ≈	**1** ≈	**2**	
Uptake via PTS	Oxidase Inhibitor	**5** >	**6** >>> **3** ≥	**4**			
CD spectra:	Low salt	**6** >	**4** >	**3** >	**2** >	**1**	
DNA Unwinding	High salt	**6** >	**4** >	**3** >	**2** >	**1**	
EtBr displacement:	Low salt	**6** >>	**5** >>	**4** >>	**3** >>	**2** >>	**1**
Apparent binding constant (K_{app})	High salt	**6** >	**4** >	**5** >	**3** >	**2** >	**1**
UV-visible titration:	Low salt	**2** >	**4** >	**3** ≈	**6** >	**1**	
DNA binding constant (K_b)[#]	High salt	**6** >	**5** >	**4** ≈	**3** ≈	**2** >	**1**
UV-visible titration:	Low salt	**6** >	**5** >	**4** ≈	**3** ≈	**2** >	**1**
Hypochromicity % at λ_{max}	High salt	**6** >	**5** >	**3** >	**4** ≈	**2** >	**1**
Gel shift analysis	Low salt, dark	**6** >	**5** >	**4** ≈	**3** >>> **2** >	**1**	

[#]Need to be revised

λ_{max} for **1** to **4** = 387 nm λ_{max} for **5** and **6** = 394 nm

REFERENCES

1.	Harrington, K. J., Biology of cancer. *Medicine* **2011,** *39* (12), 689-692.
2.	Harrington, K.; Jankowska, P.; Hingorani, M., Molecular biology for the radiation oncologist: The 5Rs of radiobiology meet the hallmarks of cancer. *Clinical Oncology* **2007,** *19* (8), 561-571.
3.	Bodduluru, L. N.; Kasala, E. R.; Madhana, R. M. R.; Sriram, C. S., Natural killer cells: The journey from puzzles in biology to treatment of cancer. *Cancer Letters* **2015,** *357* (2), 454-467.
4.	Culp, S. J.; Gaylor, D. W.; Sheldon, W. G.; Goldstein, L. S.; Beland, F. A., A comparison of the tumors induced by coal tar and benzo[a]pyrene in a 2-year bioassay. *Carcinogenesis* **1998,** *19* (1), 117-124.
5.	Boström, C.-E.; Gerde, P.; Hanberg, A.; Jernström, B.; Johansson, C.; Kyrklund, T.; Rannug, A.; Törnqvist, M.; Victorin, K.; Westerholm, R., Cancer risk assessment, indicators, and guidelines for polycyclic aromatic hydrocarbons in the ambient air. *Environmental Health Perspectives* **2002,** *110* (Suppl 3), 451-488.
6.	Mastrangelo, G.; Fadda, E.; Marzia, V., Polycyclic aromatic hydrocarbons and cancer in man. *Environmental Health Perspectives* **1996,** *104* (11), 1166-1170.
7.	Talaska, G.; Underwood, P.; Maier, A.; Lewtas, J.; Rothman, N.; Jaeger, M., Polycyclic aromatic hydrocarbons (PAHs), nitro-PAHs and related environmental compounds: Biological markers of exposure and effects. *Environmental Health Perspectives* **1996,** *104*, 901-906.
8.	Eisler, R., Polycyclic aromatic hydrocarbon hazards to fish, wildlife, and invertebrates: A synoptic review. *Contaminant Hazard Reviews* **1987,** *11*.
9.	Geacintov, N. E.; Cosman, M.; Hingerty, B. E.; Amin, S.; Broyde, S.; Patel, D. J., NMR solution structures of stereoisomeric covalent polycyclic aromatic carcinogen−DNA adducts: principles, patterns, and diversity. *Chemical Research in Toxicology* **1997,** *10* (2), 111-146.
10.	Guengerich, F. P., Metabolism of chemical carcinogens. *Carcinogenesis* **2000,** *21* (3), 345-351.
11.	Lin, C. H.; Huang, X. W.; Kolbanovskii, A.; Hingerty, B. E.; Amin, S.; Broyde, S.; Geacintov, N. E.; Patel, D. J., Molecular topology of polycyclic aromatic carcinogens determines DNA adduct conformation: A link to tumorigenic activity. *Journal of Molecular Biology* **2001,** *306* (5), 1059-1080.
12.	Alderden, R. A.; Mellor, H. R.; Modok, S.; Hambley, T. W.; Callaghan, R., Cytotoxic efficacy of an anthraquinone linked platinum anticancer drug. *Biochemical Pharmacology* **2006,** *71* (8), 1136-1145.
13.	Gibson, D.; Binyamin, I.; Haj, M.; Ringel, I.; Ramu, A.; Katzhendler, J., Anthraquinone intercalators as carrier molecules for second-generation platinum anticancer drugs. *European Journal of Medicinal Chemistry* **1997,** *32* (10), 823-831.
14.	Shi, J.; Tang, C. W., Anthracene derivatives for stable blue-emitting organic electroluminescence devices. *Applied Physics Letters* **2002,** *80* (17), 3201-3203.
15.	Janossy, I.; Kosa, T., Influence of anthraquinone dyes on optical reorientation of nematic liquid-crystals. *Optics Letters* **1992,** *17* (17), 1183-1185.
16.	Holmes, F. A.; Esparza, L.; Yap, H. Y.; Buzdar, A. U.; George, R.; Blumenschein; Hortobagyi, G. N., A comparative study of bisantrene given by two dose schedules in patients with metastatic breast cancer [abstract]. *Cancer Chemotherapy and Pharmacology* **1986,** *18* (2), 157-161.

17.   de Bono, J. S.; Oudard, S.; Ozguroglu, M.; Hansen, S.; Machiels, J. P.; Kocak, I.; Gravis, G.; Bodrogi, I.; Mackenzie, M. J.; Shen, L.; Roessner, M.; Gupta, S.; Sartor, A. O., Prednisone plus cabazitaxel or mitoxantrone for metastatic castration-resistant prostate cancer progressing after docetaxel treatment: a randomised open-label trial. *Lancet* **2010,** *376* (9747), 1147-54.

18.   Lown, J. W., Anthracycline and anthraquinone anticancer agents - current status and recent developments. *Pharmacology and Therapeutics* **1993,** *60* (2), 185-214.

19.   Parker, C.; Waters, R.; Leighton, C.; Hancock, J.; Sutton, R.; Moorman, A. V.; Ancliff, P.; Morgan, M.; Masurekar, A.; Goulden, N.; Green, N.; Revesz, T.; Darbyshire, P.; Love, S.; Saha, V., Effect of mitoxantrone on outcome of children with first relapse of acute lymphoblastic leukaemia (ALL R3): an open-label randomised trial. *Lancet* **2010,** *376* (9757), 2009-2017.

20.   Rodger, A.; Blagbrough, I. S.; Adlam, G.; Carpenter, M. L., DNA-binding of a spermine derivative - spectroscopic study of anthracene-9-carbonyl-N^1-spermine with poly d(G-C)'(d(G-C) and poly d(A-T)'d(A-T). *Biopolymers* **1994,** *34* (12), 1583-1593.

21.   Phanstiel, O. I.; Kaur, N.; Delcros, J. G., Structure-activity investigations of polyamine-anthracene conjugates and their uptake via the polyamine transporter. *Amino Acids* **2007,** *33* (2), 305-313.

22.   Rodger, A.; Taylor, S.; Adlam, G.; Blagbrough, I. S.; Haworth, I. S., Multiple DNA-binding modes of anthracene-9-carbonyl-N^1-spermine. *Bioorganic & Medicinal Chemistry* **1995,** *3* (6), 861-872.

23.   Sugiyama, S.; Vassylyev, D. G.; Matsushima, M.; Kashiwagi, K.; Igarashi, K.; Morikawa, K., Crystal structure of PotD, the primary receptor of the polyamine transport system in Escherichia coli. *Journal of Biological Chemistry* **1996,** *271* (16), 9519-9525.

24.   Muth, A.; Kamel, J.; Kaur, N.; Shicora, A. C.; Ayene, I. S.; Gilmour, S. K.; Phanstiel, O., Development of polyamine transport ligands with improved metabolic stability and selectivity against specific human cancers. *Journal of Medicinal Chemistry* **2013,** *56* (14), 5819-5828.

25.   Porter, C. W.; Miller, J.; Bergeron, R. J., Aliphatic chain length specificity of the poly amine transport system in ascites l-1210 leukemia cells. *Cancer Research* **1984,** *44* (1), 126-128.

26.   Igarashi, K.; Kashiwagi, K., Characteristics of cellular polyamine transport in prokaryotes and eukaryotes. *Plant Physiology and Biochemistry* **2010,** *48* (7), 506-512.

27.   Cullis, P. M.; Green, R. E.; Merson-Davies, L.; Travis, N., Probing the mechanism of transport and compartmentalisation of polyamines in mammalian cells. *Chemistry & Biology* **1999,** *6* (10), 717-729.

28.   Phanstiel, O. t.; Kaur, N.; Delcros, J. G., Structure-activity investigations of polyamine-anthracene conjugates and their uptake via the polyamine transporter. *Amino Acids* **2007,** *33* (2), 305-13.

29.   Bachrach, U., Naturally occurring polyamines: interaction with macromolecules [abstract]. *Current Protein & Peptide Science* **2005,** *6* (6), 559-66.

30.   Terry, C. A.; Fernandez, M. J.; Gude, L.; Lorente, A.; Grant, K. B., Physiologically relevant concentrations of NaCl and KCl increase DNA photocleavage by an N-substituted 9-aminomethylanthracene dye. *Biochemistry* **2011,** *50* (47), 10375-10389.

31.   Armitage, B. A., Cyanine dye-DNA interactions: Intercalation, groove binding, and aggregation. In *DNA Binders and Related Subjects*, Waring, M. J.; Chaires, J. B., Eds. Springer-Verlag Berlin: Berlin, 2005; Vol. 253, pp 55-76.

32.   Blackburn, G. M., Reversible small molecule-nucleic acid interactions. In *Nucleic Acids in Chemistry and Biology*, 3 ed.; Gait, M. J.; Loakes, D.; Williams, D. M., Eds. IRL Press at Oxford University Press: Oxford, England, 2006; pp 341-382.

33.   Panagiotidis, C. A.; Artandi, S.; Calame, K.; Silverstein, S. J., Polyamines alter sequence-specific DNA-Protein interactions. *Nucleic Acids Research* **1995,** *23* (10), 1800-1809.

34.   Hooper, G.; Dick, D. A., Nonuniform distribution of sodium in the rat hepatocyte. *The Journal of General Physiology* **1976,** *67* (4), 469-74.

35.   Moore, R. D.; Morrill, G. A., A possible mechanism for concentrating sodium and potassium in the cell nucleus. *Biophysical Journal* **1976,** *16* (5), 527-33.

36.   Naora, H.; Naora, H.; Mirsky, A. E.; Allfrey, V. G., Magnesium and calcium in isolated cell nuclei. *The Journal of General Physiology* **1961,** *44* (4), 713-742.

37.   Williamson, J. R.; Raghuraman, M. K.; Cech, T. R., Monovalent cation-induced structure of telomeric DNA the g-quartet model. *Cell* **1989,** *59* (5), 871-880.

38.   McFail-Isom, L.; Sines, C. C.; Williams, L. D., DNA structure: cations in charge? *Current Opinion in Structural Biology* **1999,** *9* (3), 298-304.

39.   Hooper, G.; Dick, D. A., Nonuniform distribution of sodium in the rat hepatocyte. *The Journal of general physiology* **1976,** *67* (4), 469-74.

40.   Dick, D. A., The distribution of sodium, potassium and chloride in the nucleus and cytoplasm of Bufo bufo oocytes measured by electron microprobe analysis. *The Journal of Physiology* **1978,** *284*, 37-53.

41.   Qu, X. G.; Chaires, J. B., Analysis of drug-DNA binding data. *Numerical Computer Methods, Part C* **2000,** *321*, 353-369.

42.   Cain, B. F.; Baguley, B. C.; Denny, W. A., Potential antitumor agents. 28. Deoxyribonucleic acid polyintercalating agents. *Journal of Medicinal Chemistry* **1978,** *21* (7), 658-68.

43.   Tan, W. B.; Bhambhani, A.; Duff, M. R.; Rodger, A.; Kumar, C. V., Spectroscopic identification of binding modes of anthracene probes and DNA sequence recognition. *Photochemistry and Photobiology* **2006,** *82* (1), 20-30.

44.   Duff, M. R.; Mudhivarthi, V. K.; Kumar, C. V., Rational design of anthracene-based DNA binders. *Journal of Physical Chemistry B* **2009,** *113* (6), 1710-1721.

45.   Hall, H. K., Correlation of the base strengths of amines[1]. *Journal of the American Chemical Society* **1957,** *79* (20), 5441-5444.

46.   Garbett, N. C.; Hammond, N. B.; Graves, D. E., Influence of the amino substituents in the interaction of ethidium bromide with DNA. *Biophysical Journal* **2004,** *87* (6), 3974-3981.

47.   Wilson, W. D.; Wang, Y.-H.; Kusuma, S.; Chandrasekaran, S.; Boykin, D. W., The effect of intercalator structure on binding strength and base-pair specificity in DNA interactions. *Biophysical Chemistry* **1986,** *24* (2), 101-109.
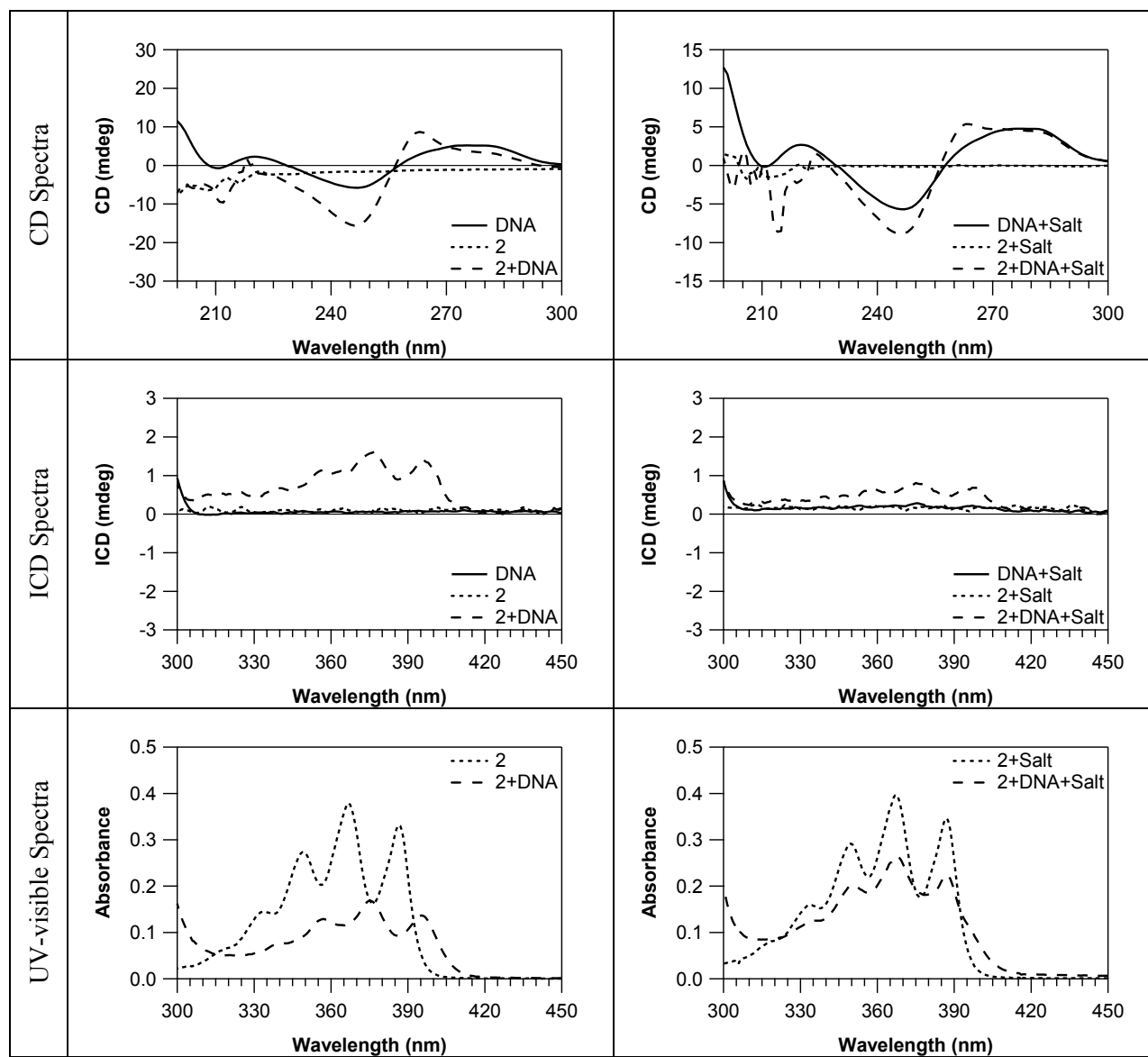
APPENDICES

Appendix A: CD, ICD, and UV-visible spectra
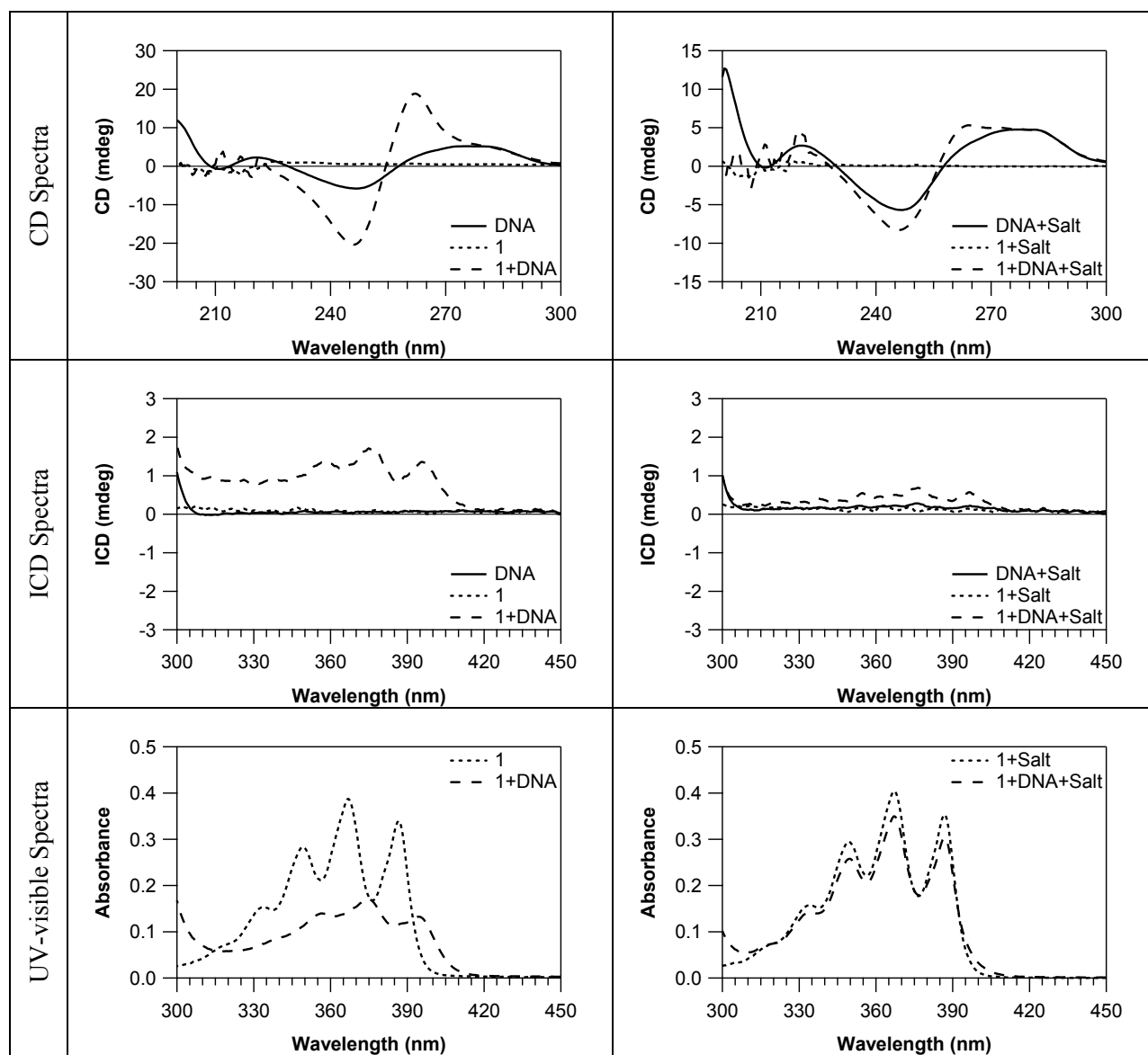
Figure A1. CD, ICD, UV-visible Spectra of **1** under low salt (10 mM sodium phosphate buffer) and high salt condition (10 mM sodium phosphate buffer, 150 mM NaCl, and 260 mM KCl)
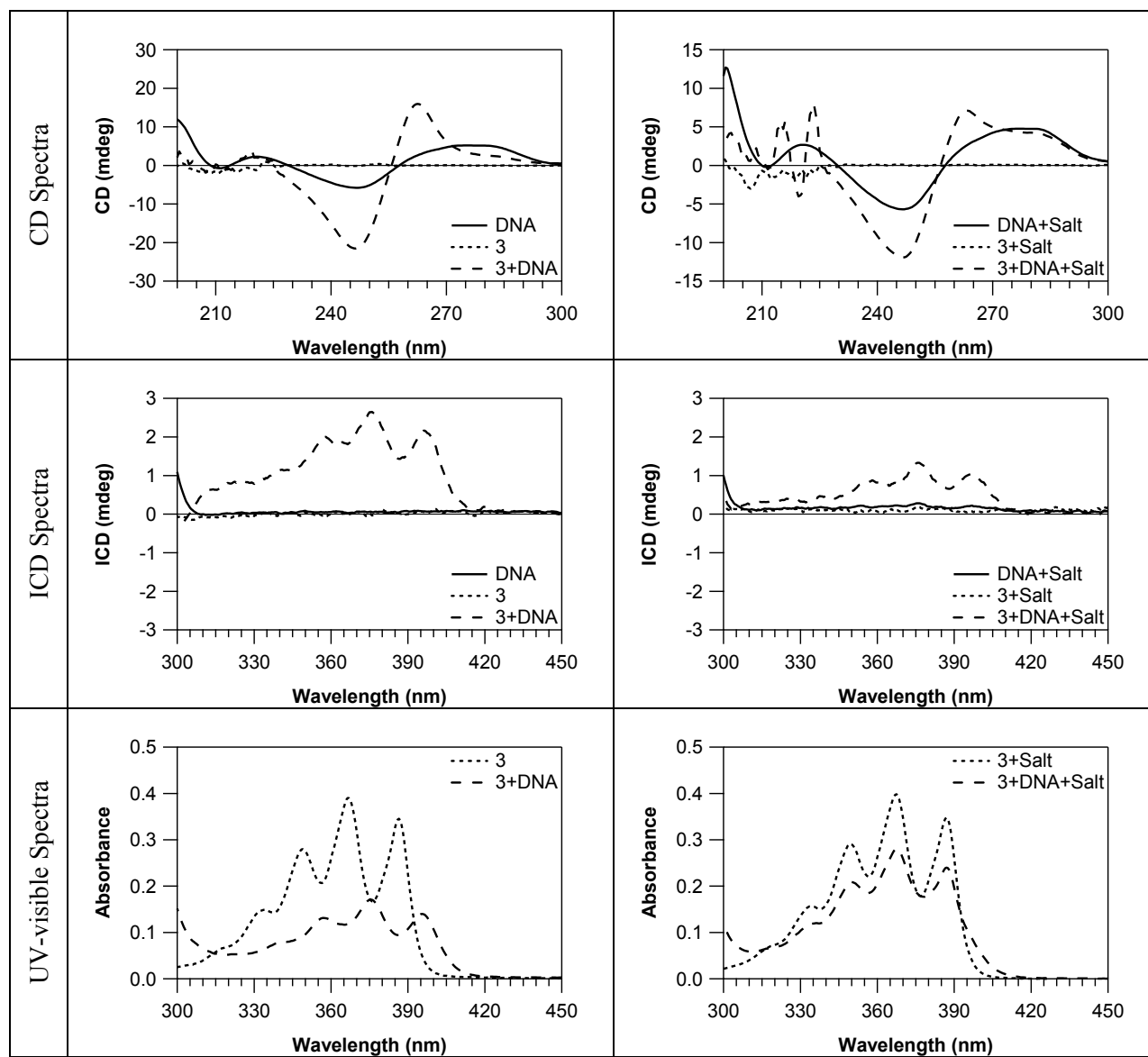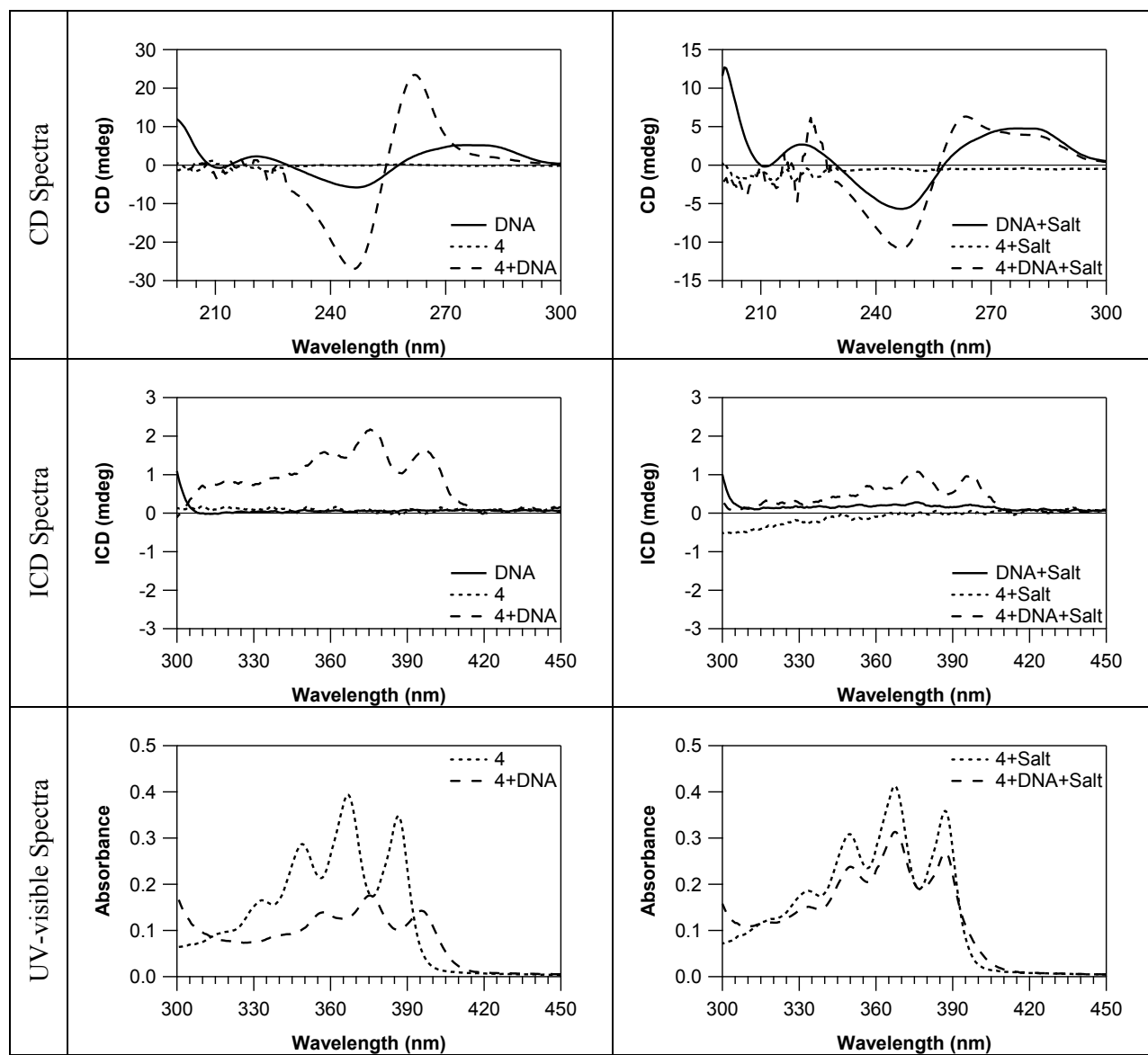CD and ICD: Ratio of [Ant]/[DNA] = 0.3
UV-visible Spectra: the **1** + DNA is at saturation for low salt or at similar ratio 0.3 for +Salt

Figure A2. CD, ICD, UV-visible Spectra of **2** under low salt (10 mM sodium phosphate buffer) and high salt condition (10 mM sodium phosphate buffer, 150 mM NaCl, and 260 mM KCl)
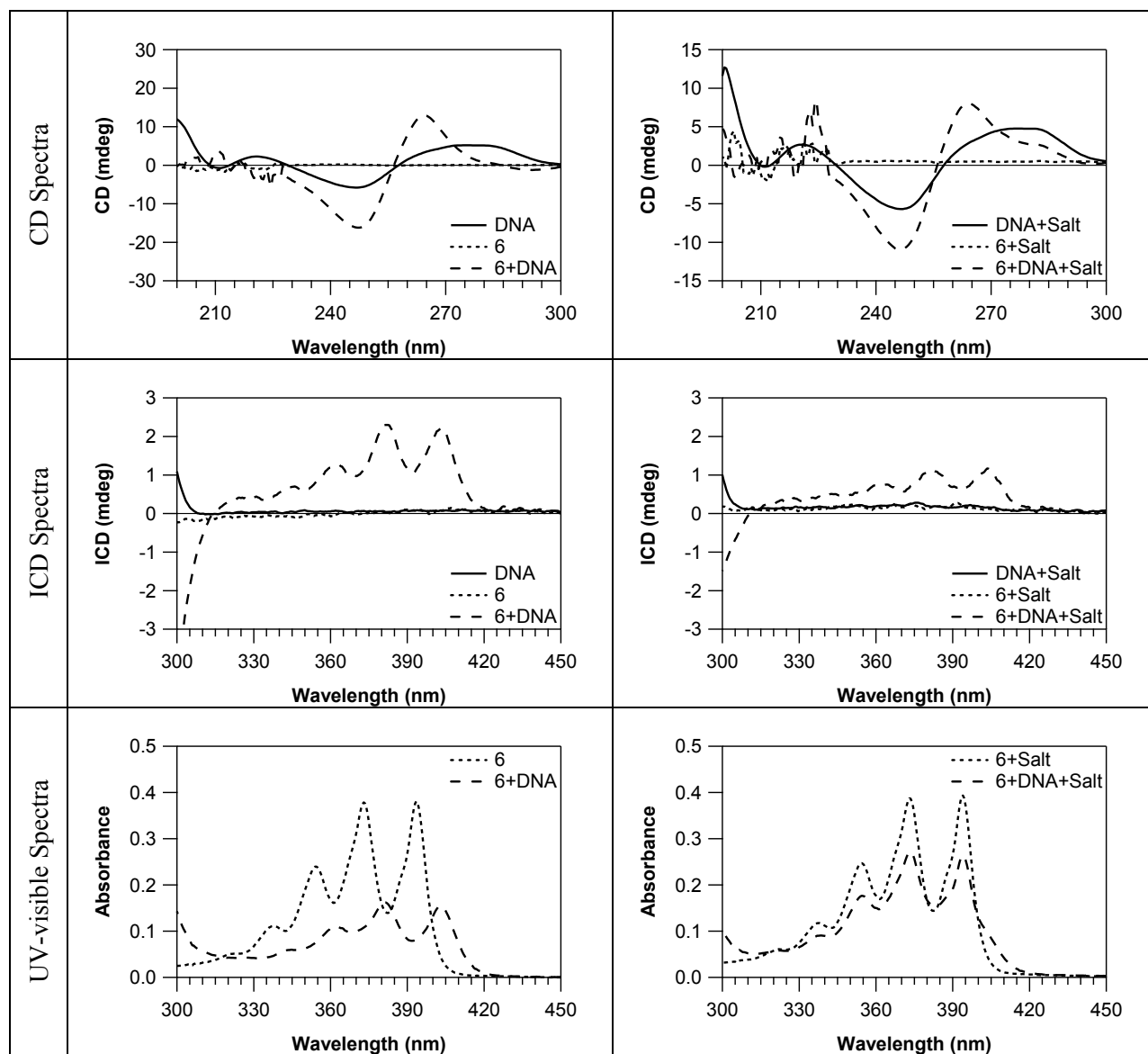CD and ICD: Ratio of [Ant]/[DNA] = 0.3
UV-visible Spectra: the **2** + DNA is at saturation for low salt or at similar ratio 0.3 for +Salt

Figure A3. CD, ICD, UV-visible Spectra of **3** under low salt (10 mM sodium phosphate buffer) and high salt condition (10 mM sodium phosphate buffer, 150 mM NaCl, and 260 mM KCl)

CD and ICD: Ratio of [Ant]/[DNA] = 0.3

UV-visible Spectra: the **3** + DNA is at saturation for low salt or at similar ratio 0.3 for +Salt

Figure A4. CD, ICD, UV-visible Spectra of **4** under low salt (10 mM sodium phosphate buffer) and high salt condition (10 mM sodium phosphate buffer, 150 mM NaCl, and 260 mM KCl)

CD and ICD: Ratio of [Ant]/[DNA] = 0.3

UV-visible Spectra: the **4** + DNA is at saturation for low salt or at similar ratio 0.3 for +Salt

Figure A5. CD, ICD, UV-visible Spectra of **6** under low salt (10 mM sodium phosphate buffer) and high salt condition (10 mM sodium phosphate buffer, 150 mM NaCl, and 260 mM KCl)

CD and ICD: Ratio of [Ant]/[DNA] = 0.3

UV-visible Spectra: the **6** + DNA is at saturation for low salt or at similar ratio 0.3 for +Salt

Appendix B: UV-visible titration spectra and Xiaogang DNA binding constant analysis

Appendix B1. Equations

Pearson's *R* (least square curve fit)

$$R = \frac{\sum_i (x_i - \bar{x})(y_i - \bar{y})}{\sqrt{\sum_i (x_i - \bar{x})^2}\sqrt{\sum_i (y_i - \bar{y})^2}};$$

x: model

y: experimental data

i: number of ith data

Xiaogang

$$A = \varepsilon_o(C_t - C_b) + \varepsilon_b C_b \qquad (1)$$
$$KC_b^2 - C_b(KD_t + KC_t + 1) + KD_tC_t = 0 \qquad (2)$$

A is the absorbance at each DNA concentration

ε_0 is the molar extinction coefficient of the free ligand
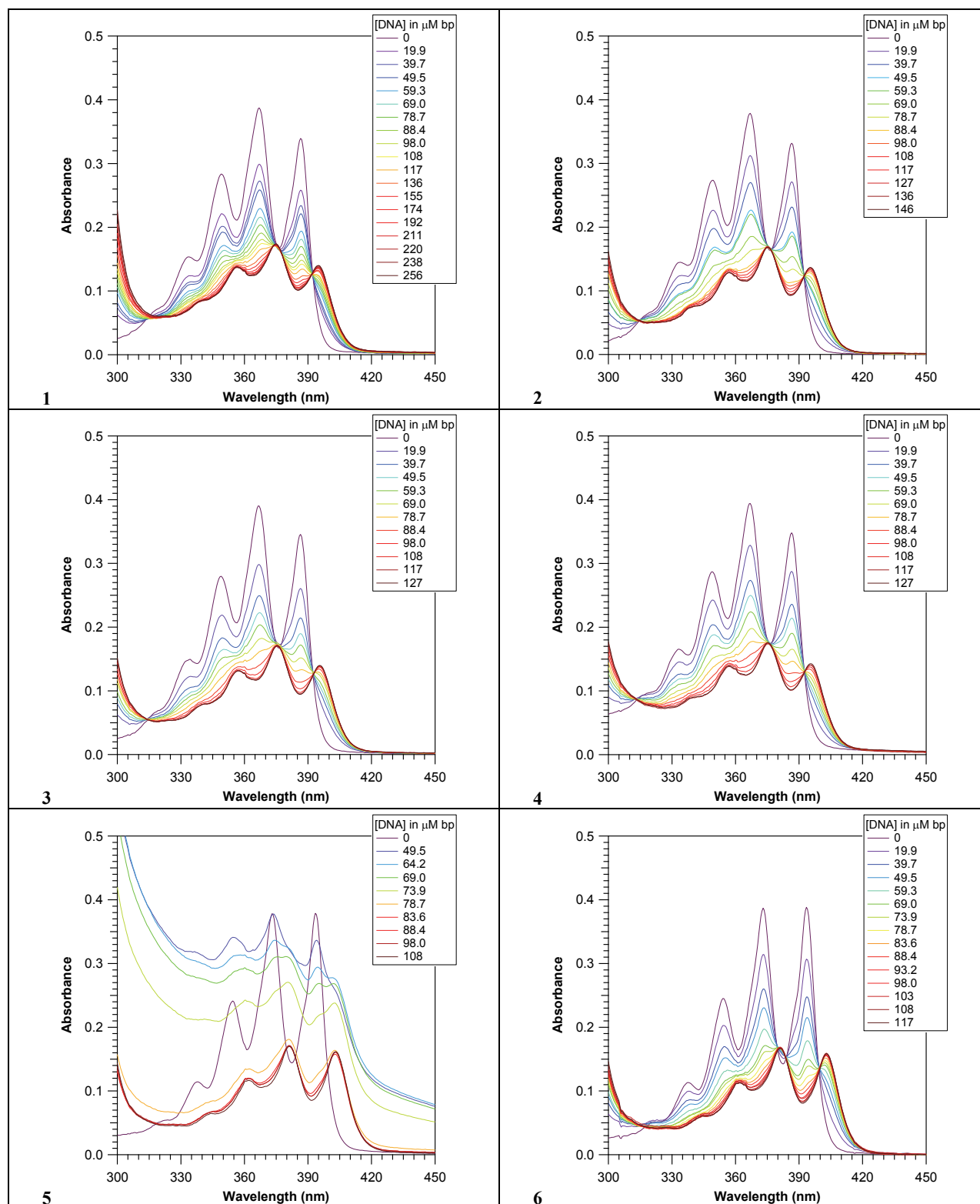
ε_b is the molar extinction coefficient of the DNA bound ligand

C_t is the total ligand concentration

C_b is the bound ligand concentration (equation 2 was solved for C_b by the quadratic formula)

D_t is the total DNA concentration, K is the DNA association constant

Appendix B2. UV-visible Spectra

Figure B1. UV-visible Spectra of Ant **1** to **6** under the low salt condition

48 µM of **1** and V_{final} = 527 µL, 85 µM of **2** and V_{final} = 515 µL, 54 µM of **3** and V_{final} = 513 µL, 48 µM of **4** and V_{final} = 513 µL, 60 µM of **5** and V_{final} = 511 µL, and 50 µM of **6** and V_{final} = 512 µL, with increasing DNA concentration under 10 mM sodium phosphate buffer (pH 7.0).
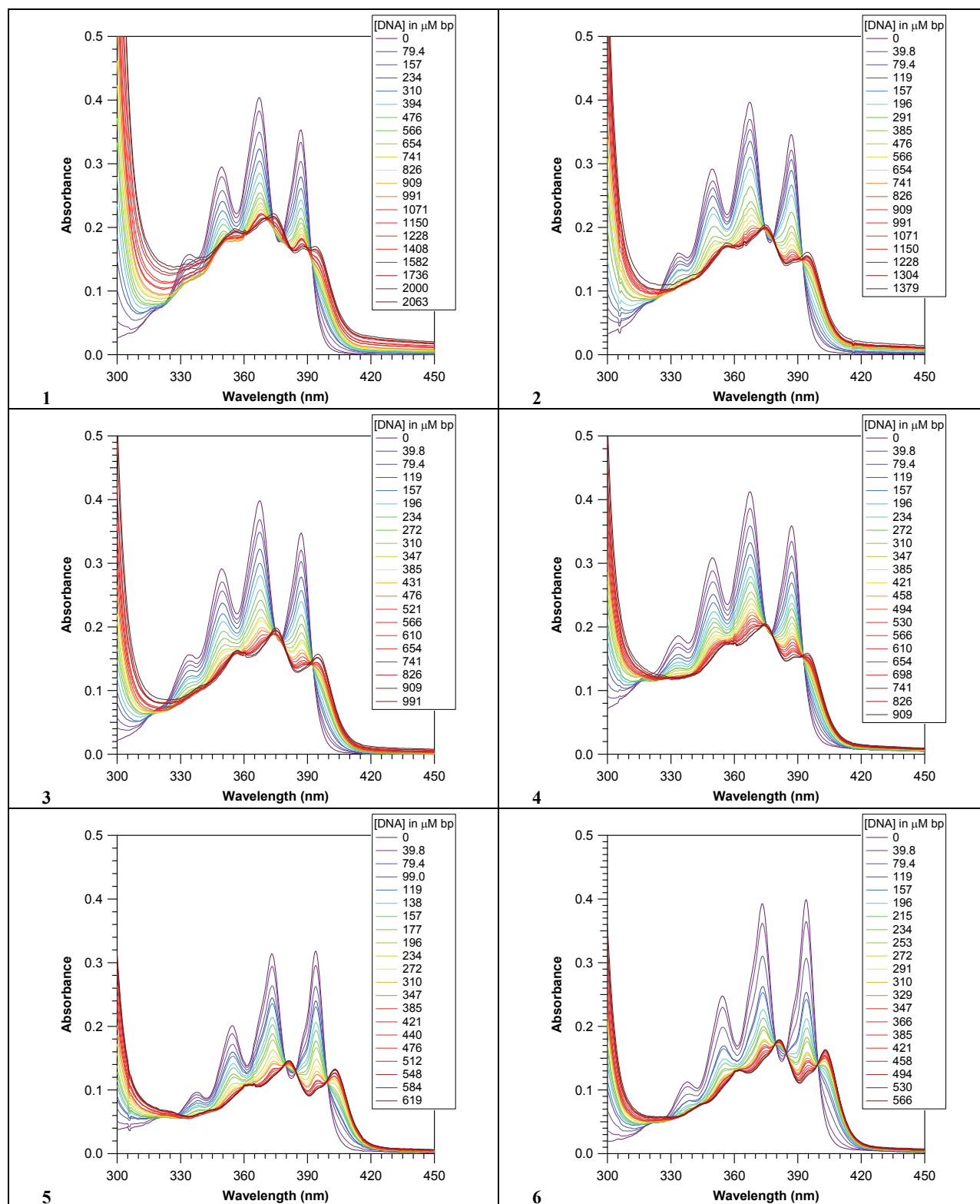
Figure B2. Representative UV-visible Spectra of Ant **1** to **6** under the high salt condition
48 µM of **1** and V_{final} = 625 µL, 85 µM of **2** and V_{final} = 580 µL, 54 µM of **3** and V_{final} = 555 µL, 48 µM of **4** and V_{final} = 550 µL, 60 µM of **5** and V_{final} = 533 µL, and 50 µM of **6** and V_{final} = 530 µL**,** with increasing DNA concentration under 10 mM sodium phosphate buffer (pH 7.0), 150 mM NaCl, and 260 mM KCl.

Appendix B3. Xiaogang Analysis
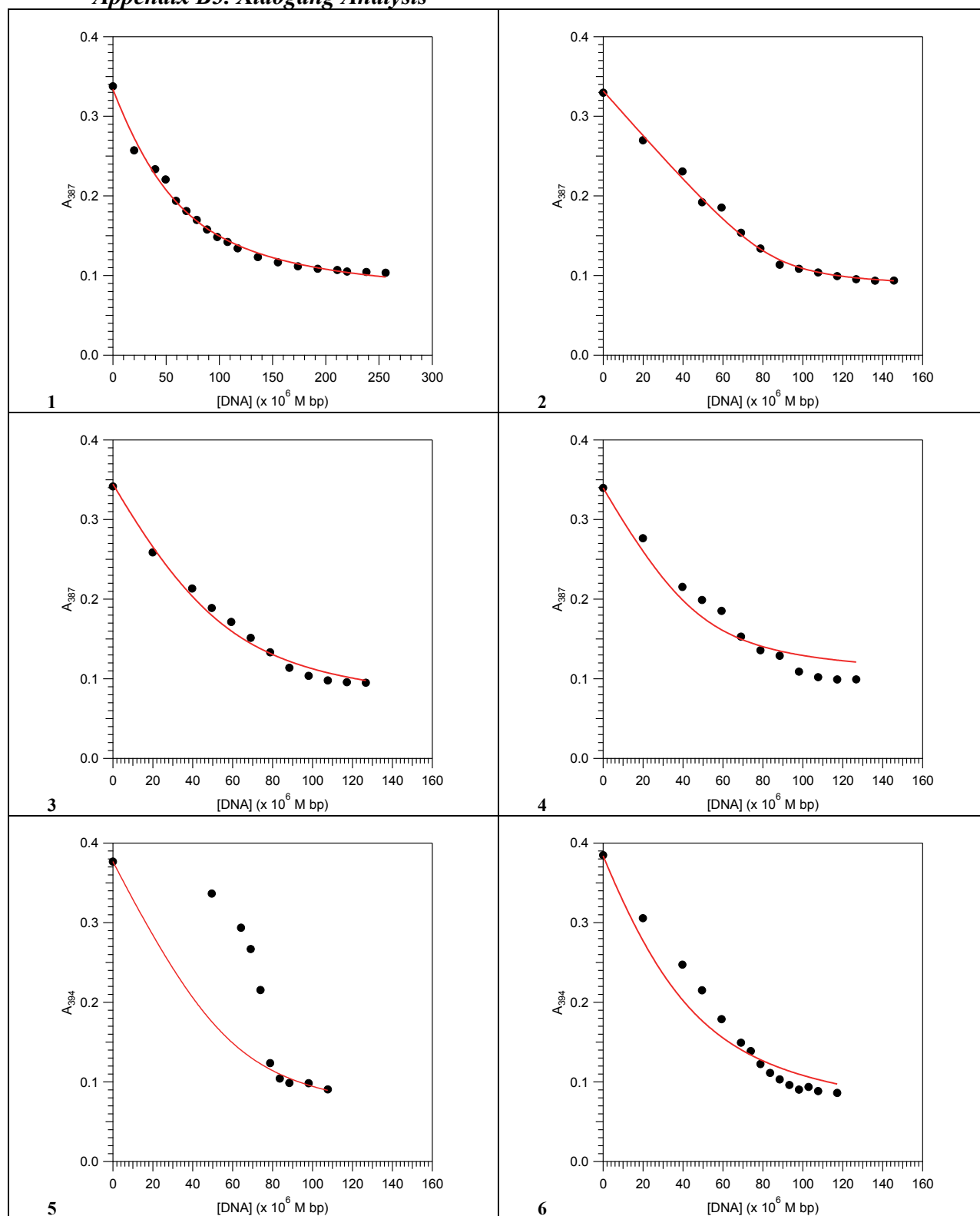
Figure B3. Xiaogang analysis of Ant **1** to **6** under the low salt condition via equations 1 and 2
Data (circle) is fitted with the Xiaogang model (solid line). Pearson's *R* value: **1** = 0.9960, **2** = 0.9976, **3** = 0.9946, **4** = 0.9785 , **5** = 0.7959 , **6** = 0.9790.
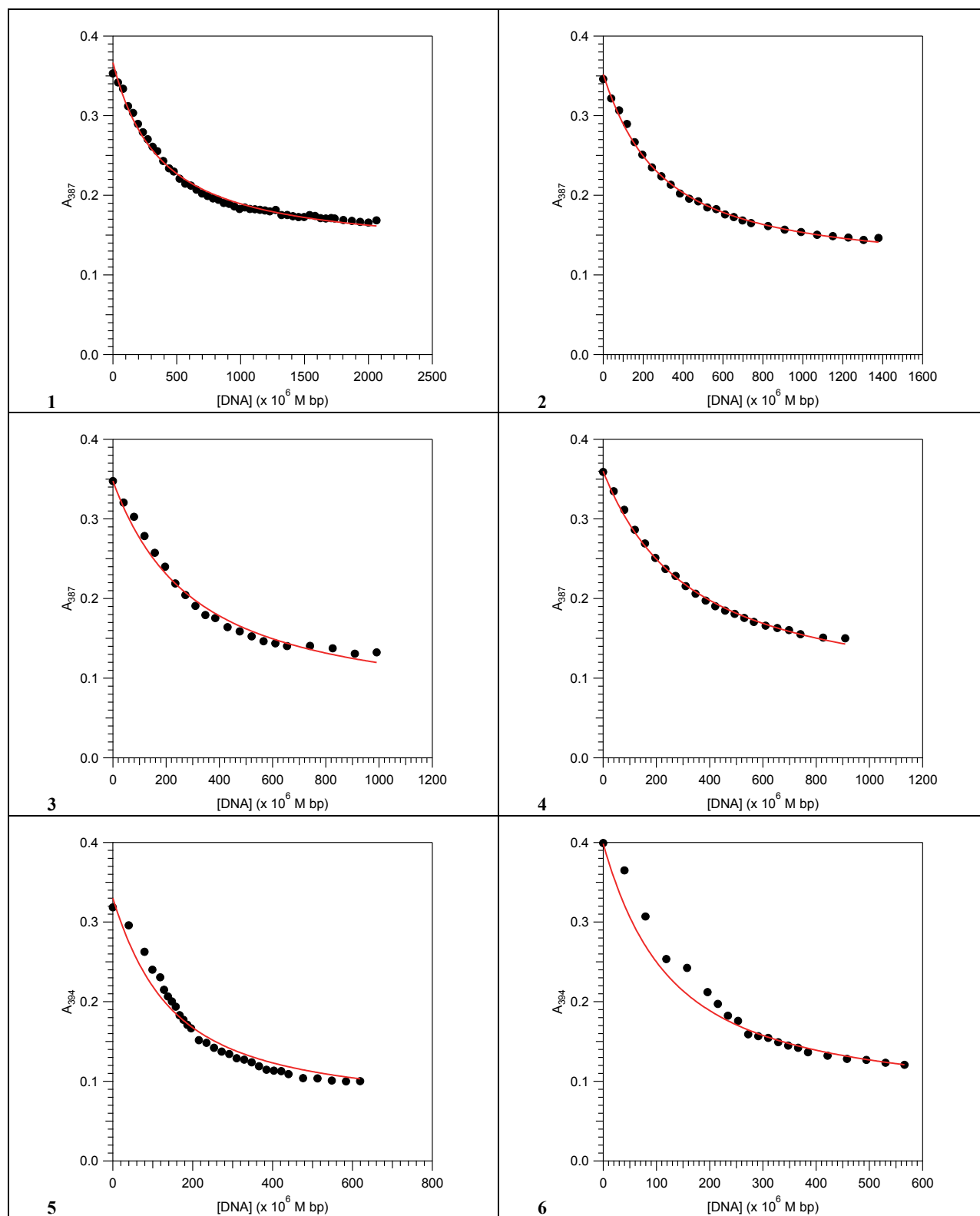
Figure B4. Xiaogang analysis of Ant **1** to **6** under the high salt condition via equations 1 and 2
Data (circle) is fitted with the Xiaogang model (solid line). Pearson's *R* value: **1** = 0.9959, **2** = 0.9988, **3** = 0.9929, **4** = 0.9982 , **5** = 0.9876 , **6** = 0.9852.

Appendix B4. Xiaogang Values

Table B4. The comparison between the real and model extinction coefficient values of free and DNA bound Ants

| Cmpd | λ_{max} (nm) | Low salt | | | | High salt | | | |
| | | Xiaogang | | Real | | Xiaogang | | Real | |
		ε_0 at λ_{max}	ε_f at λ_{max}	ε_0 at λ_{max}	ε_f at λ_{max}	ε_0 at λ_{max}	ε_f at λ_{max}	ε_0 at λ_{max}	ε_f at λ_{max}
1	387	7000 ± 115	1168 ± 141	6961 ± 65	2166 ± 13	7652 ± 561	2462 ± 165	7412 ± 399	3399 ± 154
2	387	3880 ± 39	983 ± 56	3907 ± 28	1109 ± 28	4145 ± 12	1112 ± 90	4075 ± 25	1623 ± 85
3	387	6532 ± 132	947 ± 92	6325 ± 1	1746 ± 13	6552 ± 401	1105 ± 85	6568 ± 364	2403 ± 206
4	387	7021 ± 201	1989 ± 165	7022 ± 201	2021 ± 124	7967 ± 643	1537 ± 84	7922 ± 622	3229 ± 230
5	394	$6400^{\alpha, \beta}$	$1000^{\alpha, \beta}$	$6291 \pm 19^{\beta}$	$1531 \pm 29^{\beta}$	5458 ± 19	934 ± 41	5356 ± 46	1667 ± 17
6	394	9587 ± 168	1000^{α}	9448 ± 169	2215 ± 36	9878 ± 134	1710 ± 143	9886 ± 82	2988 ± 114

$^{\alpha}$locked value $^{\beta}$n = 2

ε [M^{-1} cm^{-1}]

Real $\varepsilon_0 = \frac{A_{max}}{[Ant]}$, $\varepsilon_b = \frac{A_{min}}{[Ant]}$; [Ant] is in Table 2